A proximal radius of *Barberapithecus huerzeleri* from Castell de Barberà: Implications for locomotor diversity among pliopithecoids

Julia Arias-Martorell [a,b,*], Sergio Almécija [c,d,a], Alessandro Urciuoli [a], Masato Nakatsukasa[e], Salvador Moyà-Solà [a,f,g], David M. Alba[a,*]

[a] *Institut Català de Paleontologia Miquel Crusafont, Universitat Autònoma de Barcelona, Edifici ICTA-ICP, c/ Columnes s/n, Campus de la UAB, 08193 Cerdanyola del Vallès, Barcelona, Spain*

[b] *School of Anthropology and Conservation, Marlowe Building University of Kent, Canterbury, UK CT2 7NR, UK*

[c] *Division of Anthropology, American Museum of Natural History, Central Park West at 79th Street, New York, NY 10024, USA*

[d] *New York Consortium in Evolutionary Primatology, New York, NY 10024, USA*

[e] *Laboratory of Physical Anthropology, Graduate School of Science, Kyoto University, 606-8502 Kyoto, Japan;*

[f] *Institució Catalana de Recerca i Estudis Avançats (ICREA), Passeig de Lluís Companys 23, 08010 Barcelona, Spain*

[g] *Unitat d'Antropologia Biològica (Departament de Biologia Animal, Biologia Vegetal i Ecologia), Universitat Autònoma de Barcelona, 08193 Cerdanyola del Vallès, Barcelona, Spain*

[*]Corresponding authors.

E-mail addresses: julia.arias@icp.cat (J. Arias-Martorell); david.alba@icp.cat (D.M. Alba).

A proximal radius of *Barberapithecus huerzeleri* from Castell de Barberà: Implications for locomotor diversity among pliopithecoids

Abstract

Pliopithecoids are a diverse group of Miocene catarrhine primates from Eurasia. Their positional behavior is still unknown, and many species are known exclusively from dentognathic remains. Here we describe a proximal radius (IPS66267) from the late Miocene of Castell de Barberà (Vallès-Penedès Basin, NE Iberian Peninsula) that represents the first postcranial specimen of the pliopithecoid *Barberapithecus huerzeleri*. A body mass estimate based on the radius is compared with dental estimates, and its morphology is compared with that of extant and fossil anthropoids by qualitative means as well as by landmark-based 3D geometric morphometrics. The estimated body mass of ~5 kg for IPS66267 closely matches the dental estimates for the (female) holotype, thereby discounting an alternative attribution to the large-bodied hominoid recorded at Castell de Barberà. In multiple features (oval and moderately tilted head with a pronounced lateral lip and a restricted articular area for the capitulum; proximodistally expanded proximal radioulnar joint; and short, robust and anteroposteriorly compressed neck) the specimen differs from hominoids and resembles instead extant non-ateline monkeys and stem catarrhines. The results of the morphometric analysis further indicate that the *Barberapithecus* proximal radius shows closer similarities with non-suspensory arboreal cercopithecoids and the dendropithecid *Simiolus*. From a locomotor viewpoint, the radius of *Barberapithecus* lacks most of the features functionally related to climbing and/or suspensory behaviors and displays instead a proximal radioulnar joint that would have been particularly stable under pronation. On the other hand, the *Barberapithecus* radius differs from other stem catarrhines in the less anteroposteriorly compressed and less tilted radial head with a deeper capitular fovea, suggesting a somewhat enhanced mobility at the elbow joint. We conclude that pronograde arboreal quadrupedalism

was the main component of the locomotor repertoire of *Barberapithecus* but that, like other crouzeliids, it might have displayed better climbing abilities than pliopithecids.

Keywords: Crouzeliidae; Pliopithecidae; Fossil primates; Miocene; Functional morphology; Locomotion.

1. Introduction

Pliopithecoids are a diverse group of early to late Miocene primates that is customarily considered a Eurasian clade of stem catarrhines more derived than propliopithecoids (Andrews et al., 1996; Begun, 2002, 2017; Harrison, 2005, 2013; Urciuoli et al., 2021). Although pliopithecoids must have originated in Africa sometime during the Oligocene, their African forerunners are uncertain (Harrison, 2013; Begun, 2017)—Rossie and MacLatchy (2006) considered that *Lomorupithecus* from the early Miocene of Uganda is a pliopithecoid, but we concur with Harrison (2010, 2013) that it is more likely a dendropithecid. Undoubted pliopithecoids are not recorded until 18–17 Ma in China (Harrison and Gu, 1999; Begun, 2002, 2017; Harrison, 2013), slightly predating the earliest record of Eurasian hominoids (Heizmann and Begun, 2001; Casanovas-Vilar et al., 2011; Roos et al., 2019; Gilbert et al., 2020a). Although the internal phylogeny of the group is unclear, we provisionally classify the various pliopithecoid genera (see in particular Harrison and Gu, 1999; Moyà-Solà et al., 2001; Begun, 2002, 2017; Harrison, 2005, 2013; Alba et al., 2010; Alba and Moyà-Solà, 2012; Alba and Berning, 2013; Sankhyan et al., 2017; Harrison et al., 2020) into four different families following Harrison et al. (2020): Dionysopithecidae, Pliopithecidae, Crouzeliidae and Krishnapithecidae.

In the Iberian Peninsula, pliopithecoids are restricted to the middle and late Miocene of the Vallès-Penedès Basin (Marigó et al., 2014). They include (for details about the age, see Casanovas-Vilar et al., 2011, 2016a, 2016b; Alba et al., 2017, 2019): Pliopithecoidea indet.

from Abocador de Can Mata (ACM) locality ACM/C3-B2 (12.1 Ma; Alba et al., 2012a); "*Pliopithecus*" sp. from Sant Quirze (~11.9–11.2 Ma; Harrison et al., 2002a); the pliopithecid *Pliopithecus canmatensis* from several ACM localities from 11.9 to 11.7 Ma (Alba et al., 2010; Alba and Moyà-Solà, 2014); Crouzeliidae indet. from Can Feliu (probably <11.2 Ma; Crusafont-Pairó and Golpe-Posse, 1981); the crouzeliid *Barberapithecus huerzeleri* from Castell de Barberà (~11.2 Ma; Alba and Moyà-Solà, 2012); and the crouzeliid *Egarapithecus narcisoi* from Torrent de Febulines (9.1 Ma; Moyà-Solà et al., 2001). Both *Barberapithecus* and *Egarapithecus* were considered pliopithecids instead of crouzeliids by Begun (2002, 2017), but respectively crouzeliine and anapithecine crouzeliids by Harrison et al. (2020), and we concur with the latter view, in agreement with the original descriptions of these genera (Moyà-Solà et al., 2001; Alba and Moyà-Solà, 2012). The Vallès-Penedès pliopithecoids are mostly known from dentognathic material, which hampers making locomotor inferences. Only a few undescribed postcranial remains of *P. canmatensis* from ACM (three partial phalanges, a partial metatarsal V, a femur and a humerus shaft fragments) were preliminary reported by Alba and Moyà-Solà (2014). This contrasts with the partial skeleton of *Pliobates cataloniae*, a small-bodied catarrhine from ACM locality ACM/C8-A4 (~11.6 Ma; Alba et al., 2015, 2017) that preserves abundant postcranial elements and shows an intriguing mixture of plesiomorphic (stem catarrhine-like) and derived (crown hominoid-like) features. *Pliobates* was recovered as a stem hominoid by the cladistic analysis performed by Alba et al. (2015), but alternate cladistic analyses have suggested pliopithecoid affinities (Nengo et al., 2017; Gilbert et al., 2020a, 2020b; see also Benefit and McCrossin, 2015). While the hominoid-like features displayed by *Pliobates* in the elbow and wrist might be convergent, it shows greatest dental similarities with dendropithecids rather than pliopithecoids (Alba et al., 2015). Therefore, we refrain from including *Pliobates* in the Pliopithecoidea, pending more detailed analyses of its craniodental and postcranial morphology (currently underway).

Elsewhere in Eurasia, the postcranial anatomy of pliopithecids is best known based on three partial skeletons (one almost complete) of *Epipliopithecus vindobonensis* (included in *Pliopithecus* by some authors; e.g., Harrison et al., 2020) from the middle Miocene of Devínska Nová Ves, Slovakia (Zapfe and Hürzeler, 1957; Zapfe, 1958, 1961). The postcranial evidence for *Pliopithecus* s.s. is much more limited, including a metacarpal II, a calcaneus and a proximal pedal phalanx of *Pliopithecus antiquus* from the middle Miocene of Sansan, France (Zapfe and Hürzeler, 1957; Zapfe, 1961; Senut, 2012), and a metacarpal I (Depéret, 1887: Pl. XIII Fig. 56; Zapfe and Hürzeler, 1957; Zapfe, 1961) and a proximal humerus (Ginsburg and Mein, 1980; Arias-Martorell et al., 2015) from La Grive-Saint-Alban, France. The postcranial remains of crouzeliids are also scarce and mostly limited to anapithecines, including a manual proximal phalanx of *Laccopithecus robustus* from the late Miocene of Lufeng, China (Meldrum and Pan, 1988), as well as some phalanges and two femora of *Anapithecus hernyaki* from the late Miocene of Rudabánya, Hungary (Begun, 1988, 1993, 2002; Kordos and Begun, 1999, 2001). The currently known postcranials of crouzeliines only include a talus and a calcaneus of *Crouzelia auscitanensis* from Sansan (Senut, 2012). The femur of *Paidopithex rhenanus* from the late Miocene of Eppelsheim, Germany (Kaup, 1861; Pohlig, 1895; Begun, 1992; Köhler et al., 2002) is also considered to belong to a large pliopithecoid of uncertain affinities (Begun, 2002, 2017).

Here we describe a fragment of proximal radius (IPS66267) of a small-bodied catarrhine primate from the earliest Vallesian (MN9, late Miocene) site of Castell de Barberà (Vallès-Penedès Basin, NE Iberian Peninsula). The specimen was found among the collections of the Institut Català de Paleontologia Miquel Crusafont (ICP) in February 2012 by Lars van den Hoek Ostende while revising the uncatalogued micromammal material from this site. The specimen was mixed with other (non-primate) bone fragments in a box labeled with the name of the site but without associated museum records about the collection date or exact stratigraphic provenance. However, in all probability the specimen was collected by

Miquel Crusafont-Pairó's team during the late 1960s or 1970s, when systematic excavations were performed at the site (Alba et al., 2019). Castell de Barberà is one of the few sites where pliopithecoids and hominoids co-occur (Andrews et al., 1996; Sukselainen et al., 2015; Alba et al., 2019; DeMiguel et al., 2021). In particular, both the crouzeliine *B. huerzeleri* and a large-bodied dryopithecine (cf. *Dryopithecus fontani*) have been reported from this site (Crusafont Pairó and Hürzeler, 1969; Crusafont-Pairó and Golpe-Posse, 1981; Moyà-Solà et al., 2005; Almécija et al., 2011, 2012; Alba et al., 2011, 2019; Alba, 2012; Alba and Moyà-Solà, 2012; Marigó et al., 2014). The aim of this paper is threefold: (1) to provide a description of IPS66267; (2) to estimate the body mass of the taxon to which it belongs; and (3) to morphologically compare it, both qualitatively and quantitatively (by means of three-dimensional geometric morphometrics [3DGM]) with extant anthropoids and extinct stem catarrhines, in order to investigate its closer morphometric affinities and draw locomotor inferences. We did not include *Pliobates* in the comparative analyses because its phylogenetic position is controversial (see above) and also because its complete radius merits a deeper analysis (including both the proximal and the distal epiphyses), which are beyond the scope of this paper and will be provided in a forthcoming paper (Arias-Martorell et al., in prep.). Our results indicate that an assignment of IPS66267 to *B. huerzeleri* is warranted, thereby representing one of the few postcranial elements (and the first elbow joint element) currently available for crouzeliids. Based on morphofunctional considerations, the implications of IPS66267 for understanding locomotor diversity among the Pliopithecoidea are discussed.

2. Materials and methods

2.1. Studied and comparative sample

The proximal radius fragment from Castell de Barberà (IPS66267; Fig. 1) is housed in the ICP. A 3D model of the specimen is available from MorphoSource.org (Supplementary Online Material [SOM] File S1). Its morphology was qualitatively compared with extant and

extinct anthropoids based on 3D models, casts housed in the ICP, and the literature. The comparative fossil sample for qualitative comparisons included the following species, selected as representative fossils from their respective groups:

(a) Stem catarrhines from Africa (dendropithecids): KNM-MO 63 from Moruorot (Rose et al., 1992: Fig. 8; Senut, 1989: Fig. 62; Rossie et al., 2012) and KNM-MO 17022B from Kalodirr locality 751 (Rose et al., 1992: Fig. 9), assigned to *Simiolus enjiessi*; KNM-RU 2098 from Rusinga Island (Le Gros Clark and Thomas, 1951: Pl. 4 fig. 9, Pl. 5 fig. 11; Senut, 1989: Fig. 76, Pl. X), assigned to *Dendropithecus macinnesi*;

(b) Stem catarrhines from Europe (pliopithecoids): The radii of individuals I (catalog No. O. E. 304 PCe) and II (catalog No. NHMW 1970/1397/0003) from Devínska Nová Ves (Zapfe, 1958: Pl. 1A, B; Zapfe, 1961: Fig. 54; Senut, 1989: Fig. 95, Pl. XV), assigned to *E. vindobonensis*;

(c) Stem hominoids: KNM-RU 2036AI (left radius; Napier and Davis, 1959: Pl. 6 Fig. 20g, Pl. 7 Figs. 22–24) and 2036CE (right proximal radius; Walker and Pickford, 1983: Fig. 4; Senut, 1989: Fig. 74, Pl. VII) from Rusinga Island, assigned to *Ekembo heseloni* (see McNulty et al., 2015); KNM-TH 28860-J (proximal right radius; Ward et al., 1999: Fig 2k; Sherwood et al., 2002: Fig. 1f) from locality BPRP122 at Kipsaramon in the Tugen Hills, assigned to *Equatorius africanus*; and KNM-WK 16950J (proximal left radius; Leakey and Leakey, 1986; Leakey et al., 1988: Fig. 5) from Kalodirr, assigned to *Turkanapithecus kalakolensis*.

(d) Fossil great apes: RUD 66 from Rudabánya (Morbeck, 1983: Fig. 2D), assigned to *Rudapithecus hungaricus*; AS95.503 from Sinap locality 12 (Kappelman et al., 2003: Fig. 4.26), assigned to *Ankarapithecus meteai;* TNA 0001 (partial proximal right radius; Lin et al, 1987: Fig.1; Harrison et al., 2002b) from the Shihuiba site in Lufeng County, Yunnan Province, assigned to *Lufengpithecus lufengensis.*

We also performed quantitative analyses using 3DGM, which include an extant anthropoid sample of 117 3D models from 17 genera (Table 1; SOM Table S1). The 3D models were produced using a NextEngine surface scanner (NextEngine, Inc., California, USA) and two different high-resolution μCT scanners (SOM Table S1): a BIR ACTIS 225/300 industrial μCT scanner (Department of Human Evolution, Max Planck Institute for Evolutionary Anthropology, Germany) and a Nikon XT 225 ST μCT scanner (Cambridge Biotomography Centre, Department of Zoology, University of Cambridge, UK). Specimens scanned with the NextEngine scanner were obtained using a resolution of >10,000 points per square inch; 6–12 scans were taken at two or more positions and then merged using ScanStudio HD PRO software v. 1.3.2 (Next Engine, Santa Monica). The isotropic voxel size range for the μCT scans sample is 21.9–51.5 μm. Laser scan-derived 3D models were cleaned (fill holes, irregularities in mesh, etc.) using Geomagic Wrap 2017 (3D Systems, Inc. Morrisville), and μCT scans were processed in AVIZO v. 6.3 (Visualization Sciences Group, Berlin). 3D models obtained using different scanning techniques have been shown to produce reliable and repeatable measurements (Tocheri et al., 2011; Shearer et al., 2017). Therefore, all models were analyzed using the same software and methodology (IDAV Landmark Editor v. 3.6; Wiley et al., 2005) irrespective of digitalization techniques. To assess the reliability of high-quality casts for identifying the features described in the landmark protocol, a high-quality cast of IPS667267 was landmarked and included alongside the original specimen in the 3DGM analyses. Both fall very close to one another in the morphospace (SOM Fig. S1; SOM Table S2), suggesting that the effect of relying on casts instead of original fossil specimens is negligible for the purposes of our study.

The fossil sample for 3DGM analyses included a subsample (based on the 3D surfaces available to us) of the extinct taxa included in the qualitative assessment: the small-bodied stem catarrhines *S. enjiessi* (KNM-MO 63 and KNM-MO 17022B), *D. macinnesi* (KNM-RU 2098), and *E. vindobonensis* (O. E. 203 PCe); and *Ek. heseloni* (KNM-RU 2036AI), which

was included to adequately calibrate the stem hominoid condition. The *Simiolus* and *Epipliopithecus* specimens were scanned from high-quality casts housed at the ICP: KNM-RU 2098 and KNM-RU 2036CE (*D. macinnesi* and *Ek. heseloni*, respectively, which are both housed in the National Museums of Kenya in Nairobi, Kenya) and IPS66267 (housed at the ICP), which were scanned from the original specimens. All 3D models of the fossil material were obtained using a NextEngine surface laser scanner using the HD3 macro mode and landmarked alongside the extant sample in Landmark Editor.

2.2. Body mass estimation

Body mass (BM, in kg) was estimated for IPS66267 based on radial head surface area (RHSA, in mm^2) using the 'total sample' (cercopithecoids + hominoids) allometric equation reported by Ruff (2003: Table 7). Following Ruff (2002: Appendix Table 1), RHSA was computed as 0.785 × RHML × RHAP, where RHML and RHAP are radial head mediolateral and anteroposterior breadths (Ruff, 2002: Appendix Fig. 1). Logarithmic detransformation bias (Smith, 1993) was corrected using the quasimaximum likelihood estimator provided by Ruff (2003: Table 3) and the 95% CI for the prediction was calculated based on the standard error of estimate (SEE) and an inverse Student's t distribution with the degrees of freedom provided by the same author.

BM was also estimated for the (female) holotype of *B. huerzeleri* (IPS1724) based on the dental measurements. Following Egi et al. (2004), only first and second upper and lower molars were used. These dental BM estimates were derived from Egi et al.'s (2004: Table 2) anthropoid allometric equations based on occlusal area (mm^2). The latter was computed as the product between mesiodistal length and buccolingual width as reported by Alba and Moyà-Solà (2012), by averaging left and right antimeres when available. Logarithmic detransformation bias was corrected using the ratio estimator as reported by Egi et al. (2004: Table 2). The 95% CIs for the prediction based on each tooth were computed using the SEE

and an inverse Student's t distribution with the degrees of freedom determined by effective sample size as reported by Egi et al. (2004). An average BM estimate was then computed for IPS1724 based on the mean estimate and the maximum and minimum 95% CIs for the four molars.

2.3. Geometric morphometric analyses

The shape affinities of the proximal radius of IPS66267 were explored using 14 3D surface landmarks (Table 2; Fig. 2) on a sample of extant anthropoid radii including all extant hominoid genera (Table 1; SOM Table S1). The landmark protocol was designed specifically to capture the most informative elements of shape preserved in IPS66267, which is missing part of the posteromedial aspect of the radial head (see Section 3.1. below for a full description of preservation; Fig. 1). Therefore, no landmarks were placed in the posterior and medial aspects of the radial head or the distally extending posteromedial articular surface.

Regarding the orientation of the radii for type II and III landmark identification, complete radii (i.e., those included in the extant sample, as well as the fossil specimen of *E. vindobonensis*) were anatomically oriented in anterior view, which readily allowed the identification of the medial, lateral and posterior aspects of the radial head. The partial fossil specimens were oriented based on the anterior position of the radial tuberosity, which was preserved in all individuals and allowed us to anatomically identify the anterior aspect of the radius. Some of the landmarks had been used in previous studies, such as some of those placed on the deepest point of the fovea and outline of the radial head (Tallman, 2010, 2013). We added additional landmarks that account for the position and size of the fovea relative to the radial head outline, which has direct implications for the discrimination between cercopithecoids and hominoids (Rose 1987; Rose et al., 1992), and landmarks on the distal expansion of the articular surface of the radial head, which clearly separates hominoids from other taxa (Harrison, 1987), and on the radial neck, which is also a known aspect of variation

between hominoids, cercopithecoids, platyrrhines and fossil taxa (Rose et al., 1992). The coordinates were translated, rotated and size-scaled to unit centroid size (CS) using a generalized Procrustes analysis (GPA) with the 'Morpho' v. 2.8 package (Schlager, 2017) in R v. 3.6.1. (R Core Team, 2019). To identify major patterns of shape variation across the sample, we performed a between-group principal component analysis (bgPCA; Mitteroecker and Bookstein, 2011) on the GPA-transformed coordinates of the extant sample, with major anthropoid clades (platyrrhines, cercopithecines, colobines, hylobatids, and hominids) as the grouping factor. The fossil configurations were projected a posteriori onto the morphospace generated by the bgPCA. To address the criticisms raised on the use of bgPCA on highly-multivariate data sets (as it is the case of 3DGM data; Bookstein, 2019; Cardini et al., 2019; Cardini and Polly, 2020), and to rule out the presence of spurious grouping in the sample, we computed a cross-validated bgPCA and compared the results to those of a standard bgPCA. Group mean differences were tested with a permutational analysis of variance (PERMANOVA; 1000 permutations) based on the Euclidean distances between the means, and we computed the Z-scores and the R^2 (i.e., the amount of variance explained) for group differences in the raw shape data, and the scores of both the standard and the cross-validated bgPCAs using the 'vegan' v. 2.5 package (Oksanen et al., 2020) in R. We determined the number of between-group principal components (bgPCs) with meaningful direction (i.e., those worth interpreting and keeping for subsequent analyses; Bookstein, 2014) with the 'getMeaningfulPCs' function in 'Morpho'. The correlation between meaningful bgPC scores and log-transformed CS (with natural logarithms, ln CS) was computed by means of a phylogenetic generalized least squares (PGLS) regression (Adams, 2014) using the 'geomorph' v. 3.1.1 package (Adams et al., 2020) in R.

The phylogenetic signal embedded in proximal radius shape among extant anthropoids was quantified by means of Pagel's λ (Pagel, 1999) and Blomberg's K statistics (Blomberg et al., 2003), computed for the meaningful bgPCs using the 'phytools' v. 0.6-60 package

(Revell, 2012) in R. Both Pagel's λ and Blomberg's K test the null hypothesis of no phylogenetic signal (i.e., closely related species do not resemble each other more than distant relatives) by comparing the observed data distribution to that expected under a Brownian motion model of evolution. Despite the underlying similarities, the two statistics provide different information. Pagel's λ is a scaling factor quantifying the influence of the taxa phylogenetic relatedness on the covariance matrix of the analyzed trait (Pagel, 1999; Freckleton et al., 2002): $\lambda = 1$ implies that trait covariance is exclusively influenced by the phylogeny (i.e., under a Brownian motion model of evolution), $\lambda < 1$ suggests that other factors besides phylogeny influence trait evolution, and $\lambda = 0$ is obtained when no phylogenetic correlation is found in the data. In turn, Blomberg's K informs about how well the distribution of the phylogenetic tree tips reflects the patterns of variance-covariance found in the data. Similar to the Pagel's λ statistics, $K = 0$ implies a model of evolution that closely resembles that expected under Brownian motion; for $K < 1$, the variance accumulates within the clades, with closely related taxa resembling each other less than expected, possibly as a consequence of independent evolution (i.e., homoplasy); finally, when $K > 1$, not closely related taxa are more similar than expected under a Brownian motion model of evolution, thus implying the variance accumulates among clades (as the result of stabilizing selection or architectural constraints).

We also used a phylomorphospace approach (Sidlauskas, 2008) to visualize the magnitude and direction of major patterns of shape variation along the phylogeny. This method projects a phylogenetic tree onto a given tangent space (here defined by the first two bgPCs) by estimating ancestral node scores via a maximum likelihood method for continuous characters and by using the centroid scores of the included species as the tips of the tree branches. We relied on a molecular-based time-calibrated phylogenetic tree downloaded from 10kTrees website v. 3 (Arnold et al., 2010) for the extant taxa. The extinct taxa were added according to their phylogenetic relationships as inferred by recent cladistic studies (Gilbert et

al., 2020b: Fig. 4), i.e., *S. enjiessi* and *D. macinnesi* were considered sister taxa preceding the Eurasian stem catarrhine *E. vindobonensis,* whereas *Ek. heseloni* was considered a stem hominoid; *B. huerzeleri* was included as the sister-taxon of *E. vindobonensis* based on the assumption that pliopithecoids are monophyletic (e.g., Gilbert et al., 2020b). The divergence time of the nodes for extinct taxa was arbitrarily set 1 Myr prior to the divergence between the next derived node (Almécija et al., 2019; Urciuoli et al., 2021). The tip age estimates used for the fossils were the following: *E. vindobonensis*, 14.15 Ma (average of the maximum and minimum age ranges for MN6 in central Europe; van der Meulen et al., 2011); *S. enjiessi*, 17.2 Ma (average of the ages of Kalodirr [16.7 Ma] and Moruorot [17.7 Ma]; Rose et al., 1992); *D. macinnesi*, 17.8 Ma (age of locality R3a from the Hiwegi Formation of Rusinga Island; Drake et al., 1988; Senut, 1989; Peppe et al., 2009); *Ek. heseloni*, 17.8 Ma (age of the Kulu Formation of Rusinga Island; Peppe et al., 2009); and *B. huerzeleri*, 11.2 Ma (age of Castell de Barberà; Alba et al., 2019).

3. Results

3.1. Description

IPS66267 is a 1.9 cm-long proximal fragment of a right radius (Figs. 1 and 3a, b), similar in size to those of *Simiolus enjiessi* (Fig. 3c, d) but clearly smaller than the radius of *E. vindobonensis* (Fig. 3e, f), and more closely approching in size the radii of the smallest hylobatids (Fig. 3g, h). The shaft is broken close to the proximal limit of the radial tuberosity (Figs. 1a, 3a). The specimen is generally well preserved, except for some abrasion and breakage on the posteromedial border of the radial head (Figs. 1c–e and 3b). Although this abrasion hinders a precise evaluation of the proximal radial outline, the preserved portion clearly shows that the radial head is oval (Figs. 1e and 3b), with its major diameter passing anterolaterally to posterolaterally—assuming that the radial tuberosity is roughly situated anteriorly.

The proximal articular surface for the capitulum of the humerus (Figs. 1e and 3b) is restricted, but relatively deep. The fovea is eccentrically situated toward the posteromedial portion of the radial head. The articular surface for the zona conoidea of the humerus is more extensive medially (Fig. 1d) and, especially, laterally (Fig. 1b). There is a pronounced lateral lip (Figs. 1a–c and 3a), and the bevel for articulation with the zona conoidea of the humerus is restricted to the posterolateral side of the radial head (Fig. 1b, c). The head appears to have been more elevated medially than laterally (Figs. 1a, c and 3a), although abrasion on its posteromedial portion makes it difficult to ascertain the presence of a proximally projecting tubercle (Fig. 1c, d).

The articular surface corresponding to the proximal radioulnar joint is proximodistally more extensive on the anteromedial than on the posterolateral portion of the radial head. The presence and extent of a flattened posterior region cannot be adequately ascertained due to incomplete preservation. The radial head is tilted anterolaterally relative to the proximodistal long axis of the neck, at an angle of ca. 82º. The neck is relatively wide mediolaterally (i.e., only moderately constricted relative to the head; Figs. 1a, c and 3a), but very compressed anteroposteriorly (Fig. 1b, d). Otherwise, the morphology of the radial neck cannot be properly evaluated, due to incomplete preservation (only until close to the proximal end of the tuberosity). However, the presence of a ridge along the anteromedial portion of the neck (Fig. 1a, c)—presumably corresponding to the proximal extension of the biceps muscle insertion on the bicipital tuberosity—suggests that the neck would have been quite short.

3.2. Body mass estimates

The measurements taken on the proximal radius (Table 3) yield a BM estimate of 4.9 kg (CI = 4.4–5.3 kg), which closely matches the dental BM estimate of ~5.3 kg (CI = 4.0–6.7) computed for the holotype specimen (see Table 3 for estimates derived for each molar, which largely overlap with one another).

337

338 *3.3. Qualitative comparisons*

339 The oval proximal outline of the head of IPS66267 (Figs. 1e and 3b) resembles that of
340 extant monkeys such as *Colobus* and *Cebus*, as well as extinct stem catarrhines such as
341 *Simiolus* (Fig. 3d; Rose et al., 1992). Compared with the radial head of *Epipliopithecus* (Fig.
342 3f; Zapfe, 1958, 1961), IPS66267 is somewhat less broad mediolaterally, although all the
343 above-mentioned taxa differ from the hominoid pattern characterized by roughly circular
344 radial heads (Fig. 3g, h). The restricted and eccentrically situated area for articulation with the
345 humeral capitulum in IPS66267 further resembles the morphology of both extant and extinct
346 non-hominoid anthropoids, although the fovea is somewhat deeper. This morphology suggests
347 for IPS66267 a more globular humeral capitulum than in the above-mentioned non-hominoid
348 taxa (including *Dendropithecus*, *Simiolus* and *Epipliopithecus*), although still smaller than in
349 extant and extinct hominoids. In this respect, stem hominoids such as *Ekembo*,
350 *Turkanapithecus* and *Equatorius*, as well as the fossil hominid *Lufengpithecus*, already
351 display a more derived pattern (Walker and Pickford, 1983; Leakey et al., 1988; Lin et al.,
352 1987; Rose et al., 1992; Rose, 1993a; Ward et al., 1999; Sherwood et al., 2002)—
353 characterized by more circular radial heads, as well as larger and deeper foveae—which more
354 closely resembles that in extant apes and humans.

355 The pronounced lateral lip of IPS66267 also resembles that of extant monkeys,
356 dendropithecids and *Epipliopithecus* (Rose et al., 1992). In contrast, in extant hominoids the
357 lateral lip is much less developed and more similar in size to the medial one. In this respect,
358 the stem hominoids *Ekembo, Turkanapithecus*, and *Equatorius* (Walker and Pickford, 1983;
359 Rose et al., 1992), as well as the fossil great apes *Ankarapithecus* (Kappelman et al., 2003),
360 *Rudapithecus* (Morbeck, 1983; Rose et al., 1992) and *Lufengpithecus* (Lin et al., 1987; Rose,
361 1997) show an intermediate condition (i.e., a moderately developed lateral lip). With regard to
362 the bevel for articulation with the zona conoidea, in IPS66267 it is restricted to the region of

363 the lateral lip, as in non-hominoid anthropoids (Rose et al., 1992), whereas in hominoids it
364 occupies most of the radial head contour and it is visible in side view. Stem hominoids also
365 display an intermediate condition for this feature, with a beveled area that is more extensive in
366 side view than in non-hominoid anthropoids, and which is not restricted to the lateral lip
367 (Walker and Pickford, 1983; Leakey et al., 1988; Rose et al., 1992; Sherwood et al., 2002).
368 *Ankarapithecus* and *Lufengpithecus* show a more derived pattern than stem hominoids, with
369 the bevel being well developed both anteriorly and medially (Lin et al., 1987; Rose, 1993a,
370 1997; Kappelman et al., 2003).
371 The medial elevation of the radial head (relative to its lateral portion) in IPS66267 is
372 also displayed to some degree by most anthropoids, being related to the anterolateral
373 angulation of the head relative to the neck. The development of this feature in IPS66267 is
374 intermediate between the condition displayed by non-hominoid anthropoids and that of both
375 hominoids and atelines (i.e., subfamily Atelinae, which includes the woolly and spider
376 monkeys), in which the angulation is less marked. In this respect, the similar degree of tilting
377 of the radial head in *Epipliopithecus* and *Dendropithecus* is more pronounced than that of
378 IPS66267, so that the former taxa more closely resemble the condition of most non-hominoid
379 catarrhines (Zapfe, 1961; Rose et al., 1992; Rose, 1993a, 1994). In contrast, the morphology
380 of *Ekembo, Equatorius* and *Turkanapithecus* (Walker and Pickford, 1983; Rose et al., 1992;
381 Ward et al. 1999; Sherwood et al., 2002; Leakey et al., 1988), with no medial elevation of the
382 head, resembles the extant hominoid condition much more closely than IPS66267.
383 IPS66267 shows a marked proximodistal extension of the articular surface of the
384 proximal radioulnar joint on the anteromedial portion of the radial head, compared to its
385 posterolateral portion, which is another typical feature of anthropoids—excluding atelines and
386 hominoids. Thus, IPS66267 does not differ from the condition of *Epipliopithecus* and the
387 dendropithecids *Simiolus* and *Dendropithecus* (Rose et al., 1992; Rose, 1993a). Only extinct
388 hominoids (*Ekembo, Turkanapithecus, Equatorius, Ankarapithecus* and *Lufengpithecus*)

389 approximate to some degree the extant hominoid condition, with the proximal radioulnar joint
390 occupying part of the radial head periphery (Lin et al., 1987; Leakey et al., 1988; Rose, 1997;
391 Rose et al., 1992; Sherwood et al., 2002; Kappelman et al., 2003). Similarly, the
392 mediolaterally broad but anteroposteriorly quite compressed radial neck of IPS66267 is also
393 characteristic of most anthropoids (except hominoids and atelines), including *Epipliopithecus*,
394 *Simiolus* and *Dendropithecus* (Rose et al., 1992), so that only in *Ekembo* the neck is less
395 compressed anteroposteriorly—the radial neck of *Equatorius* and *Turkanapithecus* appears to
396 be slightly more compressed than in *Ekembo* (Leakey et al., 1988; Ward et al., 1999;
397 Sherwood et al., 2002).
398
399 *3.4. Proximal radial shape analysis*
400 The bgPCA (Fig. 4) discriminates among extant hominoids, cercopithecoids and
401 platyrrhines. In particular, the analysis correctly classifies 73% of cases (70% after cross-
402 validation; SOM Fig. S2a, b) in the five groups defined a priori (platyrrhines, cercopithecines,
403 colobines, hylobatids, and hominids). Group differences were significant at $p < 0.001$
404 irrespective of whether the raw data or bgPCA (either standard or cross-validated) data were
405 analyzed. The Z-scores were similar for the raw data (8.12), standard bgPCA (10.45) and cross-
406 validated bgPCA (10.45), and R^2 increased to some extent from the raw data comparisons (0.24)
407 to cross-validated (0.46) and standard (0.46) bgPCA—overall indicating that grouping structure
408 is not spurious but that variance may also be influenced by other factor(s). bgPC3 and bgPC4
409 only accounted for <10% of variance each, were not reported back as meaningful, and yielded
410 no meaningful discrimination; therefore, only the results for bgPC1 and bgPC2 are given below.
411 bgPC1 (69% of variance) is significantly correlated with ln CS ($p = 0.001$), with great
412 apes and humans displaying the most negative values. However, CS only accounts for a
413 limited amount of shape variation ($R^2 = 0.35$, adjusted $R^2 = 0.33$), as best illustrated by the
414 fact that hylobatids and *Ateles* considerably overlap with hominids. bgPC1 embeds significant

phylogenetic signal (K = 0.42, $p = 0.004$; $\lambda = 0.73$, $p = 0.03$), but the low value of both $K < 1$ and $\lambda < 1$ suggests a considerable amount of homoplasy. Overall, this axis discriminates between hominoids (hominids with negative scores, and hylobatids with slightly negative to intermediate scores) and most monkeys (more positive scores, particularly in colobines and platyrrhines)—with the exception of *Ateles*, which partly overlaps the hominoid (particularly, hylobatid) range of variation (Fig. 4). With the exception of *Ekembo*, which occupies intermediate scores, all the other fossils including *Barberapithecus* fall squarely within the monkey distribution apart from hominoids, with *Epipliopithecus* having the most positive score among the fossils, closely followed by *Dendropithecus* (Fig. 4). Shape differences along bgPC1 are driven by the shape of the radial head (Fig. 4a–d). The more positive scores displayed by stem catarrhines and monkeys other than *Ateles* denote more oval radial heads in proximal view (Fig. 4c) and a marked medial elevation of the head in anterior view (Fig. 4d), which results into an anterolateral angulation of the head. In contrast, hominoids and *Ateles*, which display negative scores, have a more circular head (Fig. 4a) that is not tilted (Fig. 4b). Furthermore, in the groups with more positive scores the articular surface extends less distally onto the side of the head, particularly laterally and medially, while hominoids and *Ateles* have a well-developed distal expansion of the articular surface with beveling.

bgPC2 (19% of variance), which is not correlated with ln CS ($p = 0.83$), distinguishes between platyrrhines and cercopithecoids with only a slight overlap between cebids and colobines (Fig. 4). This axis embeds no significant phylogenetic signal (K = 0.18, $p = 0.60$; $\lambda = 0.27$, $p = 0.16$). *Barberapithecus* and a *Simiolus* specimen (KNM-MO 17022B) and *Ekembo* (albeit, with somewhat more negative values) occupy an intermediate position between colobines and platyrrhines, whereas the other *Simiolus* specimen (KNM-MO 63), *Epipliopithecus* and, in particular, *Dendropithecus*, show very negative scores and more closely align with platyrrhines (other than *Ateles*). Shape differences along bgPC2 are driven by the size (larger vs. smaller) and position (eccentric vs. centrally located) of the fovea

441 relative to the radial head outline, as well as its relative depth (i.e., shallower vs. deeper).
442 Specimens with positive scores have a larger, deeper, and non-eccentric (i.e., centrally placed)
443 fovea as well as a more rounded head outline (Fig. 4g), whereas specimens with negative
444 scores display a shallower, more eccentric and restricted fovea together with an oval head
445 outline (Fig. 4e). Negative scores further denote a slightly more tilted head (Fig. 4f) as
446 compared with specimens with more positive scores (Fig. 4h).
447 The phylomorphospace approach (Fig. 5) reconstructs the LCAs of crown anthropoids,
448 crown platyrrhines, and crown catarrhines as very similar to one another, being characterized
449 by positive bgPC1 and negative bgPC2 scores, and essentially displaying a non-ateline
450 platyrrhine-like morphology most similar to that of *Alouatta*. The LCA reconstructed for the
451 two analyzed pliopithecoids is virtually identical to those of crown anthropoids and crown
452 platyrrhines, and broadly similar to the dendropithecid *Simiolus* and the crown catarrhine
453 LCA. However, note that the LCA of anthropoids was left unrooted so that its position could
454 shift to some extent if stem anthropoids were incorporated into the analysis. Similarly, the
455 position of the LCAs of pliopithecoids and of *Simiolus* + crown catarrhines might slightly
456 vary depending on the divergence time arbitrarily chosen for computing their estimation.
457 *Barberapithecus* is most similar to *Cebus*, whereas *Epipliopithecus* and *Dendropithecus*
458 appear more divergent and convergent with *Lagothrix* by showing extremely positive bgPC1
459 scores. In turn, the LCA of crown cercopithecoids appears slightly derived toward more
460 positive bgPC2 scores than platyrrhines, whereas that of crown hominoids is markedly more
461 derived toward the modern ape condition (characterized by more negative scores along
462 bgPC1). The stem hominoid *Ekembo* is closely situated to the hominoid LCA and occupies an
463 intermediate position between platyrrhines and living apes along bgPC1. *Ateles* shows a
464 displacement toward negative values (i.e., toward the hominoids) in bgPC1 alongside
465 *Mandrillus*, even though they are clearly differentiated in bgPC2. Remarkably, among the

466 fossil taxa, *Dendropithecus* shows the most extreme negative scores for bgPC2 (followed
467 closely by *Epipliopithecus*).
468
469 **4. Discussion**
470 *4.1. The catarrhine elbow complex*
471 Our results indicate that the overall shape of the proximal radius is only partially
472 explained by the phylogenetic relationships among taxa because locomotor adaptation has
473 played a significant role in shaping elbow joint morphology and, specifically, the proximal
474 radius (Harrison 1987; Rose, 1993a). In particular, we found no significant phylogenetic
475 signal in bgPC2 (probably because the hominoid scatter encompasses entirely that of
476 monkeys; Fig. 4), while bgPC1 embedded significant phylogenetic signal but with low values
477 of K and λ (denoting homoplasy). To further explore these results, alternative evolutionary
478 models should be tested in the future under different phylogenetic assumptions, as our model
479 is based on the most simplistic approach.
480 Of the few analyses devoted to the proximal radius published to date, Patel (2005) did
481 not detect a functional signal in the proximal radius of extant hominoids, as they display
482 entirely similar and distinctly derived humeroantebrachial articular complexes (e.g.,
483 Sarmiento et al., 2002: Fig. 4). However, Patel (2005) relied on linear measurements and did
484 not explore the evolutionary implications of proximal radial shape in fossil apes or other
485 catarrhines except hominins, which are essentially like other extant hominoids. Tallman
486 (2010) also found poor separation between taxa in her 3DGM analysis, and attributed it to
487 intraobserver error due to reliance on type II and III landmarks around the radial head. This
488 study, however, used only four landmarks on the radial head and one on the deepest point of
489 the fovea to explore proximal radial shape, and, similarly to Patel (2005), did not include non-
490 hominoid primates in the comparative extant taxa. In contrast, our results, based on a wider
491 sample of anthropoids, have been able to identify an important role of function in the

492 proximal radius shape variation—best illustrated by the convergence in proximal radius
493 morphology between *Ateles* and hominoids, with the former overlapping the hominoid
494 morphospace in the bgPCA despite being placed in different a priori groups (see below for
495 further discussion). In the same vein, in the phylomorphospace analysis we detected a
496 considerable amount of homoplasy, which might have been at least partly brought about by
497 the morphological convergence between *Ateles* and hominoids (especially hylobatids),
498 although the results also indicate some degree of convergence between *Hylobates agilis* and
499 *Mandrillus sphinx*. Additional analyses based on a landmark protocol for the full proximal
500 radial shape would be needed to confirm and better characterize the latter apparent
501 convergence. In contrast, *Ateles* shares with hominoids a more rounded outline and deeper
502 fovea than in cercopithecoids and quadrupedal platyrrhines, as well as a less tilted head and
503 the presence of a bevel (albeit better developed in hominoids, where it encompasses the whole
504 circumference of the head) beyond the lateral lip of the radial head. Our quantitative shape
505 analyses thus agree with previous reports, based on linear measurements, that found
506 convergence between *Ateles* and hominoids in the elbow in general (Ashton et al., 1971) and
507 more specifically for proximal radial morphology, among other elements of the forelimb
508 (Takahashi, 1990; Larson 1998). The traits shared with *Ateles* are part of the derived elbow
509 joint complex characteristic of modern hominoids, which has been described extensively in
510 the literature (Rose 1988; Sarmiento et al., 2002; Patel, 2005). . The derived condition of
511 hominoids (and *Ateles*) in the proximal radius is readily reflected in our 3DGM analyses—
512 especially bgPC1, because shape differences along bgPC2 are more difficult to interpret (both
513 from a functional and a phylogenetic viewpoint). Such characteristics are functionally related
514 to wide pronation/supination ranges and, together with multiple derived features of the
515 humeroulnar joint enabling a wide range of flexion/(hyper)extension, they allow hominoids to
516 maintain considerable joint stability in a variety of elbow postures (Morbeck, 1976; Harrison,

1982; Sarmiento, 1987, 1988; Rose, 1988, 1993b; Begun, 1992; Kelley, 1997; Alba et al., 2011).

An essentially primitive elbow morphology more closely representing the ancestral anthropoid morphotype (Rose, 1988, 1993a, 1994, 1997; Senut, 1989) is reflected in both the Miocene dendropithecids from Africa (*Dendropithecus* and *Simiolus*; Le Gros Clark and Thomas, 1951; Harrison, 1982; Fleagle, 1983; Rose, 1988, 1993a, 1994, 1997; Senut, 1989; Rose et al., 1992) and the pliopithecoids from Eurasia (Zapfe, 1958, 1961; Fleagle, 1983; Rose, 1993a, 1994). The primitive catarrhine elbow complex is characterized, regarding the radius, by (1) a relatively small and flat fovea, (2) a broad peripheral lateral surface, resulting in an asymmetrical (oval) proximal outline of the radial head, and (3) an articular surface that extends distally and involves the anteromedial side of the radial head, being most suited to stability maintenance in a flexed-elbow and pronated hand posture (i.e., the load-bearing phase of quadrupedal progression; Rose, 1988).

Regarding the above, our results further support the notion that, in terms of proximal radial head, hominoids and cercopithecoids diverged in opposite directions from the ancestral anthropoid morphotype (Rose, 1988). However, paleontological evidence indicates that the hominoid elbow complex evolved in a mosaic-like, stepwise fashion (Rose, 1983, 1988, 1993a; Alba et al., 2011, 2012b, 2015). Our results highlight that the proximal radius morphology of stem hominoids such as *Ekembo*, *Turkanapithecus* and *Equatorius* is intermediate between extant hominoids and cercopithecoids (Napier and Davis, 1959; Morbeck, 1975, 1976; Harrison, 1982; Fleagle, 1983; Walker and Pickford, 1983; Rose, 1983, 1993a, 1997; Leakey et al., 1988; Sherwood et al., 2002; Begun, 2015). This intermediate morphology suggests the use of more varied elbow postures than in non-hominoid taxa, but still indicates a higher stability in full pronation (Rose, 1988, 1997; Alba et al., 2011). The radial morphology of *Ekembo* and *Turkanapithecus*, with a rounder outline of the head with less tilting and more extensive bevel, but not yet as developed as in extant hominoids, is thus

consistent with a locomotor repertoire basically relying on flexed-elbow stable positions (albeit with an enhanced stability in wide-ranging pronosupination), concordant with the slow and powerful-grasping cautious climbing/clambering and above-branch quadrupedalism typically inferred for these taxa (Fleagle, 1983; Walker and Pickford, 1983; Rose, 1983, 1988, 1993a, 1997; Leakey et al., 1988; Sarmiento, 1988, 1995; Ward, 1993, 1998, 2015; Ward et al., 1993; Rein et al., 2011). While *Equatorius* might have displayed some form of semiterrestrial locomotion (McCrossin et al., 1998; Patel et al., 2009), its radial morphology appears overall similar to that of *Ekembo* and *Turkanapithecus* (Rose, 1993a). In contrast, the elbow morphology of fossil great apes such as *Rudapithecus*, *Hispanopithecus*, *Ankarapithecus* and *Lufengpithecus* (Morbeck, 1983; Lin et al., 1987; Begun, 1992; Moyà-Solà and Köhler, 1996; Kappelman, 2003; Alba et al., 2011, 2012b) indicates the possession of a quite modern humeroantebrachial complex preserving stability through broad ranges of flexion/extension and pronation/supination postures. The modern elbow complex of these taxa would be suitable for both vertical climbing and suspensory behaviors (Begun, 1992, 1994; Rose, 1993a; Moyà-Solà and Köhler, 1996; Kappleman et al., 2003; Ward, 2015; Alba et al., 2012b), as in extant hylobatids and great apes, although still retaining some features functionally related to above-branch quadrupedalism (Alba et al., 2012b).

4.2. Locomotor inferences for Barberapithecus *and other stem catarrhines*

As noted in the original description of the species (Alba and Moyà-Solà, 2012), *B. huerzeleri* is a small-sized pliopithecoid, similar in size to *Dionysopithecus* and several *Pliopithecus* species, such as *P. canmatensis*. The BM estimated here for IPS66267 is entirely compatible with an attribution to a female individual of *B. huerzeleri.* IPS66267 shows morphological affinities with monkeys (particularly cebids and colobines) as well as the dendropithecid *Simiolus* (particularly the specimen KNM-MO 17022B), instead of hominoids, *Ateles* and stem apes, and also fits quite well the primitive catarrhine morphotype

(Rose, 1988, 1994; Rose et al., 1992). The morphological differences between the two *Simiolus* specimens (particularly in bgPC2) do not exceed the variability range of most extant genera included in the analysis. Therefore, they might simply reflect intraspecific variation, maybe related to sexual dimorphism, with IPS66267 more closely resembling the smaller radius (KNM-MO 17022B). In fact, the radial head size differences between KNM-MO 17022B and KNM-MO 63 are similar to those between male and female average values for extant taxa such as *Cebus* (Rose et al., 1992: Table 4). On the other hand, it should be taken into account that the attribution of these radii to *Simiolus* is tentative (Rose et al., 1992), so that one of them might potentially belong to a different small catarrhine genus.

Qualitatively, the proximal radius of *Barberapithecus* essentially resembles the morphology of most non-hominoid anthropoids (i.e., extant monkeys other than atelines, as well as putative stem catarrhines), in the following features: (1) relatively short and robust neck; (2) markedly compressed neck anteroposteriorly; (3) proximodistally very expanded proximal radioulnar joint on the anteromedial portion of the head; (4) pronounced lateral lip; (5) restricted beveled articular surface for the humeral capitulum; and (6) tilted radial head with an oval outline. This is also quantitatively supported by our morphometric analyses, in which the shape of radial head outline, the expanded proximal radioulnar joint on the anteromedial portion of the head, and the tilting of the head appeared as the major drivers of shape change and group separation. The proximal radius of *Barberapithecus* also displays some deviations from the primitive catarrhine elbow pattern. In particular, the radial head of *Barberapithecus* displays a deeper capitular fovea than *Dendropithecus*, *Epipliopithecus* and *Simiolus* from Moruorot, which suggests that the humeral capitulum in *Barberapithecus* might have been more globular. Similarly, *Barberapithecus* displays slightly less tilting of the radial head relative to the neck with respect to the aforementioned fossil taxa—but more markedly so than extant hominoids and stem apes. Nevertheless, *Barberapithecus* seems to possess a more intermediate condition (with respect to the other fossil catarrhines

595 *Epipliopithecus* and *Simiolus*) between the primitive catarrhine morphotype and the derived
596 condition of hominoids and stem apes.
597 From a morphofunctional viewpoint, the extensive morphological similarities between
598 the proximal radius of *Barberapithecus* and the inferred primitive condition for catarrhines
599 and even anthropoids suggest extensive humeroradial contact only when the forearm was in a
600 fully pronated position (Rose, 1988, 1994; Rose et al., 1992). Moreover, the presence of a
601 mediolaterally restricted but proximodistally extensive ulnar notch of the radius in
602 *Barberapithecus*—resembling the primitive catarrhine condition—further indicates a
603 particularly stable radioulnar articulation. These features, together with the oval and tilted
604 radial head without extensive beveling, are suitable for quadrupedal locomotion, with limb
605 movements preferentially limited along the parasagittal plane, and with restricted forearm
606 pronation/supination capabilities (Harrison, 1982; Rose, 1988, 1994; Rose et al., 1992).
607 *Barberapithecus* also displays some morphological features in the proximal radius—an
608 anteroposteriorly less compressed radial neck (based on our qualitative assessment), as well
609 as a relatively deeper capitular fovea and a less tilted head (observed both qualitatively and
610 quantitatively—that might be related to improved mobility at the elbow joint, thus suggesting
611 enhanced climbing as compared with the primitive anthropoid pattern.
612 The other investigated fossil catarrhines (*Simiolus*, *Dendropithecus* and
613 *Epipliopithecus*) appear morphologically close to the crown anthropoid and platyrrhine
614 ancestral morphotypes (Rose, 1988, 1993a, 1994, 1997; Senut, 1989). *Simiolus* has been
615 interpreted as an arboreal quadruped most similar to platyrrhines (Rose et al., 1992; Rose,
616 1993a, 1994, 1997; Harrison, 2010), and our analyses indicate closer similarities specifically
617 with *Alouatta* (characterized by a slow and deliberate pronograde locomotion with a high
618 percentage of climbing; Cant, 1986; Youlatos, 1993), suggesting that *Simiolus* might have
619 relied on a slower form of locomotion than other, more agile platyrrhines such as cebids.
620 Fleagle (1983) put forward similarities between *Dendropithecus* and *Ateles* as well, inferring

621 quadrupedalism and suspension and/or climbing for this taxon, while Rose (1988) and Rose et
622 al (1992) described the radius of *Dendropithecus* as sharing with other small fossil
623 catarrhines, such as *Simiolus*, the generalized anthropoid morphotype more suited to
624 quadrupedal locomotion and without the extensive pronosupination ranges of suspensory
625 and/or climbing of hominoids and *Ateles.* Similarly, arboreal quadrupedalism has generally
626 been inferred for *Epipliopithecus* (e.g., Bacon, 1994); however, inferences of below-branch
627 suspensory behaviors have also been made based on forelimb morphological similarities with
628 *Lagothrix* and *Ateles* (Fleagle, 1983; Conroy and Rose, 1983; Rose, 1988; Rose et al., 1992;
629 Rein et al., 2011, 2015; Arias-Martorell et al., 2015). Our analyses of proximal radial shape
630 should be contrasted with analyses on other remains preserved for these taxa. However, both
631 *Dendropithecus* and *Epipliopithecus* appear similar to each other in proximal radial
632 morphology, and derived toward the morphology of the semisuspensory *Lagothrix*, thus
633 supporting the notion these fossil catarrhines might have displayed some suspensory
634 capabilities (Fleagle, 1983: Rein et al., 2011, 2015; Arias-Martorell et al., 2015)
635 superimposed on a generalized quadrupedal locomotor repertoire.
636 Additionally, some morphological differences between *Epipliopithecus* and
637 *Pliopithecus* have been noted by previous authors (Senut, 2012; Alba and Moyà-Solà, 2014;
638 Arias-Martorell et al., 2015), although their implications in terms of positional behavior are
639 uncertain due to the scarce material available for the latter genus. Based on the Sansan
640 material, Senut (2012) concluded that both *Pliopithecus* and *Crouzelia* were semiarboreal (or
641 semiterrestrial) animals that displayed a marked quadrupedal component—with the former
642 probably showing more slow-climbing abilities, and the latter displaying more rapid arboreal
643 and/or terrestrial running. The latter behavior (most likely arboreal) cannot be discounted
644 either for *Barberapithecus*, given its morphological similarities in proximal radial shape with
645 the smaller and more agile arboreal monkeys (particularly *Cebus*). Other crouzeliid
646 postcranial remains are scarce and include phalanges and pedal elements of *Anapithecus*

hernyaki (Begun, 1988, 1993) as well as a manual proximal phalanx of *Laccopithecus robustus* (Meldrum and Pan, 1988). The phalanges of *Anapithecus* are generally similar to those of *Epipliopithecus*, but further display some features (e.g., a more marked curvature) indicative of climbing and/or suspensory postures (Begun, 1993). The phalangeal morphology of *Laccopithecus* is more hylobatid-like, thus suggesting even more marked suspensory adaptations than in *Anapithecus* (Meldrum and Pan, 1988). Postcranial elements from other anatomical regions would be necessary for *Barberapithecus* and other pliopithecoids to better reconstruct their locomotor repertoires. However, based on currently available data, pliopithecoids overall appear to have been remarkably diverse in terms of positional behavior.

5. Summary and conclusions

We describe a proximal radial fragment (IPS66267) from the late Miocene of Castell de Barberà (11.2 Ma; Vallès-Penedès Basin, NE Iberian Peninsula) that constitutes the first known postcranial of the pliopithecoid *B. huerzeleri* (Crouzeliidae, Anapithecinae). The postcranial anatomy of crouzeliines (and hence their positional behavior) are poorly known, as is the case of other pliopithecoids with the exception of *Epipliopithecus*. IPS66267 generally resembles the proximal radius of extant anthropoids other than hominoids and *Ateles*, as well as those of dendropithecids (especially *Simiolus*). On the other hand, IPS66267 displays some features indicative of enhanced mobility at the elbow joint, suggesting that *Barberapithecus* might have displayed better climbing abilities than *Epipliopithecus* and dendropithecids. We conclude that *Barberapithecus* might thus have been a pronograde arboreal quadruped, which, like other crouzeliids, might have displayed better climbing abilities than pliopithecids. In this regard, pliopithecoids as a whole (and crouzeliids in particular) display a diversity of positional behaviors, including semiterrestrial quadrupedalism (in *Pliopithecus*, and, possibly *Crouzelia*), arboreal quadrupedalism (in *Barberapithecus*), and arboreal quadrupedalism with occasional suspensory behaviors (in

673 *Epipliopithecus*, *Anapithecus* and, probably to an even greater extent, *Laccopithecus*), thus
674 highlighting the locomotor diversity attained by these Eurasian stem catarrhines.
675
676 **Acknowledgments**
677 This work has been funded by the by the Agencia Estatal de Investigación (CGL2016-76431-
678 P and CGL2017-82654-P, AEI/FEDER EU; and BES-2015-071318 to A.U.), the Generalitat
679 de Catalunya/CERCA Programme, and the Agència de Gestió d'Ajust Universitaris i de
680 Recerca of the Generalitat de Catalunya (2017 SGR 86 and 2017 SGR 116 GR, and Beatriu de
681 Pinós Programme-H2020 MSCA-Cofund Grant No 801370 to J.A.M). We thank Lars van den
682 Hoek Ostende and Isaac Casanovas-Vilar for drawing our attention to the proximal radius
683 fragment described in this paper, and Marta Palmero for the artwork. We are also thankful to
684 the Editor (Clément Zanolli), the Associate Editor (Terry Harrison), and three anonymous
685 reviewers for useful comments and suggestions that helped to improve this paper.
686
687 **References**
688 Adams, D.C., 2014. A method for assessing phylogenetic least squares models for shape and
689 other high-dimensional multivariate data. Evolution 68, 2675–2688.
690 Adams, D. C., Collyer, M.L., Kaliontzopoulou, A., 2020. Geomorph: Software for geometric
691 morphometric analyses. R package version 3.2.1. https://cran.r-
692 project.org/package=geomorph.
693 Alba, D.M., 2012. Fossil apes from the Vallès-Penedès Basin. Evol. Anthropol. 21, 254–269.
694 Alba, D.M., Berning, B., 2013. On the holotype and original description of the pliopithecid
695 *Plesiopliopithecus lockeri* (Zapfe, 1960). J. Hum. Evol. 65, 338–340.
696 Alba, D.M., Moyà-Solà, S., 2012. A new pliopithecid genus (Primates: Pliopithecoidea) from
697 Castell de Barberà (Vallès-Penedès Basin, Catalonia, Spain). Am. J. Phys. Anthropol. 147,
698 88–112.

699 Alba, D.M., Moyà-Solà, S., 2014. New fossil remains of *Pliopithecus canmatensis* from
700 Abocador de Can Mata, and their implications for the taxonomic validity and phylogenetic
701 position of *Epipliopithecus* (Primates, Pliopithecidae). Am. J. Phys. Anthropol. 153 (S58),
702 64.
703 Alba, D.M., Almécija, S., Casanovas-Vilar, I., Méndez, J.M., Moyà-Solà, S., 2012b. A partial
704 skeleton of *Hispanopithecus laietanus* from Can Feu and the mosaic evolution of crown-
705 hominoid positional behaviors. PLoS One 7, e39617.
706 Alba, D.M., Almécija, S., DeMiguel, D., Fortuny, J., Perez de los Rios, M., Pina, M., Robles,
707 J.M., Moyà-Solà, S., 2015. Miocene small-bodied ape from Eurasia sheds light on
708 hominoid evolution. Science 350, aab2625.
709 Alba, D.M., Casanovas-Vilar, I., Garcés, M., Robles, J.M., 2017. Ten years in the dump: An
710 updated review of the Miocene primate-bearing localities from Abocador de Can Mata (NE
711 Iberian Peninsula). J. Hum. Evol. 102, 12–20.
712 Alba, D.M., Garcés, M., Casanovas-Vilar, I., Robles, J.M., Pina, M., Moyà-Solà, S.,
713 Almécija, S., 2019. Bio- and magnetostratigraphic correlation of the Miocene primate-
714 bearing site of Castell de Barberà to the earliest Vallesian. J. Hum. Evol. 132, 32–46.
715 Alba, D.M., Moyà-Solà, S., Almécija, S., 2011. A partial hominoid humerus from the middle
716 Miocene of Castell de Barberà (Vallès-Penedès Basin, Catalonia, Spain). Am. J. Phys.
717 Anthropol. 144, 365–381.
718 Alba, D.M., Moyà-Solà, S., Malgosa, A., Casanovas-Vilar, I., Robles, J.M., Almécija, S.,
719 Galindo, J., Rotgers, C., Bertó Mengual, J.V., 2010. A new species of *Pliopithecus*
720 Gervais, 1849 (Primates: Pliopithecidae) from the Middle Miocene (MN8) of Abocador de
721 Can Mata (els Hostalets de Pierola, Catalonia, Spain). Am. J. Phys. Anthropol. 141, 52–75.
722 Alba, D.M., Moyà-Solà, S., Robles, J.M., Galindo, J., 2012a. Brief Communication: The
723 oldest pliopithecid record in the Iberian Peninsula based on new material from the Vallès-
724 Penedès Basin. Am. J. Phys. Anthropol. 147, 135–140.

725 Almécija, S., Alba, D.M., Moyà-Solà, S., 2011. Large-hominoid remains from the Middle
726 Miocene locality of Castell de Barberà (Vallès-Penedès Basin, Catalonia, Spain). Am. J.
727 Phys. Anthropol. 144 (S52), 74.
728 Almécija, S., Alba, D.M., Moyà-Solà, S., 2012. The thumb of Miocene apes: new insights
729 from Castell de Barberà (Catalonia, Spain). Am. J. Phys. Anthropol. 148, 436–450.
730 Almécija, S., Tallman, M., Sallam, H.M., Fleagle, J.G., Hammond, A.S., 2019. Early
731 anthropoid femora reveal divergent adaptive trajectories in catarrhine hind-limb evolution.
732 Nat. Commun. 10, 4778.
733 Andrews, P., Harrison, T., Delson, E., Bernor, R.L., Martin, L., 1996. Distribution and
734 biochronology of European and Southwest Asian Miocene catarrhines. In: Bernor, R.L.,
735 Fahlbusch, V., Mittmann, H.-W. (Eds.), The Evolution of Western Eurasian Neogene
736 Mammal Faunas. Columbia University Press, New York, pp. 168–207.
737 Arias-Martorell, J., Alba, D.M., Potau, J.M., Bello-Hellegouarch, G., Pérez-Pérez, A., 2015.
738 Morphological affinities of the proximal humerus of *Epipliopithecus vindobonensis* and
739 *Pliopithecus antiquus*: suspensory inferences based on a 3D geometric morphometrics
740 approach. J. Hum. Evol. 80, 83–95.
741 Arnold, C., Matthews, L.J., Nunn, C.L., 2010. The 10kTrees website: A new online resource
742 for primate phylogeny. Evol. Anthropol. 19, 114–118.
743 Bacon, A.-M., 1994. Nouvelles perspectives sur la locomotion de *Pliopithecus vindobonensis*
744 (Zapfe et Hüerzeler, 1957). C. R. Acad. Sci. Paris 318, 259–266.
745 Begun, D.R., 1988. Catarrhine phalanges from the Late Miocene (Vallesian) or Rudabánya,
746 Hungary. J. Hum. Evol. 17, 413–438.
747 Begun, D.R., 1992. Phyletic diversity and locomotion in primitive European hominids. Am. J.
748 Phys. Anthropol. 87, 311–340.
749 Begun, D.R., 1993. New catarrhine phalanges from Rudabánya (Northeastern Hungary) and
750 the problem of parallelism and convergence in hominoid postcranial morphology. J. Hum.

751 Evol. 24, 373–402.
752 Begun, D.R., 1994. Relations among the great apes and humans: new interpretations based on
753 the fossil great ape *Dryopithecus*. Yrbk. Phys. Anthropol. 37, 11–63.
754 Begun, D.R., 2002. The Pliopithecoidea. In: Hartwig, W.C. (Ed.), The Primate Fossil Record.
755 Cambridge University Press, Cambridge, pp. 221–240.
756 Begun, D.R., 2015. Fossil record of Miocene hominoids. In: Henke, W., Tattersall, I. (Eds.),
757 Handbook of Paleoanthropology, 2nd ed. Springer, Heidelberg, pp. 1261–1332.
758 Begun, D.R., 2017. Evolution of the Pliopithecoidea. In: Fuentes, A. (Ed.), The International
759 Encyclopedia of Primatology. John Wiley & Sons,
760 https://doi.org/10.1002/9781119179313.wbprim0165.
761 Benefit, B.R., McCrossin, M.L., 2015. A window into ape evolution. Science 350, 515–516.
762 Blomberg, S.P., Garland, T., Ives, A.R., 2003. Testing for phylogenetic signal in comparative
763 data: behavioral traits are more labile. Evolution 57, 717–745.
764 Bookstein, F. L., 2014. Measuring and Reasoning: Numerical Inference in the Sciences.
765 Cambridge University Press, Cambridge.
766 Bookstein, F.L., 2019. Pathologies of between-groups principal components analysis in
767 geometric morphometrics. Evol. Biol. 46, 271–302.
768 Bookstein, F.L., Schaefer, K., Prossinger, H., Seidler, H., Fieder, M., Stringer, C., Weber,
769 G.W., Arsuaga, J.-L., Slice, D., Rohlf, J.F., Recheis, W., Mariam, A.J., Marcus, L.F., 1999.
770 Comparing frontal cranial profiles in archaic and modern *Homo* by morphometric analysis.
771 Anat. Rec. 257, 217–224.
772 Cant, J. G. H., 1986. Locomotion and feeding postures of spider and howling monkeys: Field
773 study and evolutionary interpretation. Folia Primatol. 46, 1–14.
774 Cardini, A., Polly, P.D., 2020. Cross-validated between group PCA scatterplots: A solution to
775 spurious group separation? Evol. Biol. 47, 85–95.
776 Cardini, A., O'Higgins, P., Rohlf, F.J., 2019. Seeing distinct groups where there are none:

Spurious patterns from between-group PCA. Evol. Biol. 46, 303–316.
Casanovas-Vilar, I., Alba, D.M., Garcés, M., Robles, J.M., Moyà-Solà, S., 2011. Updated chronology for the Miocene hominoid radiation in Western Eurasia. Proc. Natl. Acad. Sci. USA 108, 5554-5559.
Casanovas-Vilar, I., Garcés, M., Van Dam, J., García-Paredes, I., Robles, J.M., Alba, D.M., 2016b. An updated biostratigraphy for the late Aragonian and the Vallesian of the Vallès-Penedès Basin (Catalonia). Geol. Acta 14, 195–217.
Casanovas-Vilar, I., Madern, A., Alba, D.M., Cabrera, L., García-Paredes, I., Van den Hoek Ostende, L.W., DeMiguel, D., Robles, J.M., Furió, M., Van Dam, J., Garcés, M., Angelone, C., Moyà-Solà, S., 2016a. The Miocene mammal record of the Vallès-Penedès Basin (Catalonia). C. R. Palevol 15, 791–812.
Conroy, G.C., Rose, M.D., 1983. The evolution of the primate foot from the earliest primates to the Miocene hominoids. Foot Ankle 3, 342–363.
Crusafont-Pairó, M., Golpe-Posse, J.M., 1981. Estudio de la dentición inferior del primer pliopitécido hallado en España (Vindoboniense terminal de Castell de Barberà, Cataluña, España). Butll. Inf. Inst. Paleontol. Sabadell 13, 25–38.
Crusafont Pairó, M., Hürzeler, J., 1969. Catálogo comentado de los póngidos fósiles de España. Acta Geol. Hisp. 4(2), 44–48.
DeMiguel, D., Domingo, L., Sánchez, I.M., Casanovas-Vilar, I., Robles, J.M., Alba, D.M., 2021. Palaeoecological differences underlie rare co-occurrence of Miocene European primates. BMC Biology 9, 6.
Depéret, C., 1887. Recherches sur la succession des faunes de Vertébrés Miocènes de la Vallée du Rhone. Arch. Mus. Hist. Nat. Lyon 4, 46–313.
Egi, N., Takai, M., Shigehara, N., Tsubamoto, T., 2004. Body mass estimates for Eocene eosimiid and amphipithecid primates using prosimian and anthropoid scaling models. Int. J. Primatol. 25, 211–236.

803 Fleagle, J.G., 1983. Locomotor adaptations of Oligocene and Miocene hominoids and their
804 phyletic implications. In: Ciochon, R.L., Corruccini, R.S. (Eds.), New Interpretations of
805 Ape and Human Ancestry. Plenum Press, New York, pp. 301–324.
806 Freckleton, R.P., Harvey, P.H., Pagel, M., 2002. Phylogenetic analysis and comparative data:
807 a test and review of evidence. Am. Nat. 160, 712–726.
808 Gilbert, C.C., Ortiz, A., Pugh, K.D., Campisano, C.J., Patel, B.A., Singh, N.P., Fleage, J.G.,
809 Patnaik, R., 2020b. New middle Miocene ape (Primates: Hylobatidae) from Ramnagar,
810 India fills major gaps in the hominoid fossil record. Proc. R. Soc. B 287, 20201655.
811 Gilbert, C.C., Pugh, K.D., Fleagle, J.G., 2020a. Dispersal of Miocene hominoids (and
812 pliopithecoids) from Africa to Eurasia in light of changing tectonics and climate. In:
813 Prasad, G.V., Patnaik, R. (Eds.), Biological Consequences of Plate Tectonics. New
814 Perspectives on Post-Gondwana Break-Up—A Tribute to Ashok Sahni. Springer, Cham,
815 pp. 393–412.
816 Ginsburg, L., Mein, P., 1980. *Crouzelia rhodanica*, nouvelle espèce de Primate catarhinien, et
817 essai sur la position systématique des Pliopithecidae. Bull. Mus. Natl. Hist. Nat. Paris 4,
818 57–85.
819 Harrison, T., 1982. Small-bodied apes from the Miocene of East Africa. Ph.D. Dissertation,
820 University College London, London.
821 Harrison, T., 1987. The phylogenetic relationships of the early catarrhine primates: a review
822 of the current evidence. J. Hum. Evol. 16, 41–80.
823 Harrison, T., 2005. The zoogeographic and phylogenetic relationships of early catarrhine
824 primates in Asia. Anthropol. Sci. 113, 43–51.
825 Harrison, T., 2010. Dendropithecoidea, Proconsuloidea, and Hominoidea (Catarrhini,
826 Primates). In: Werdelin, L., Sanders, W.J. (Eds.), Cenozoic Mammals of Africa. University
827 of California Press, Berkeley, pp. 429–469.
828 Harrison, T., 2013. Catarrhine origins. In: Begun, D.R. (Ed.), A Companion to

829 Paleoanthropology. Blackwell Publishing, Chichester, pp. 377–396.
830 Harrison, T., Gu, Y., 1999. Taxonomy and phylogenetic relationships of early Miocene
831 catarrhines from Sihong, China. J. Hum. Evol. 37, 225–277.
832 Harrison, T., van der Made, J. Ribot, F., 2002a. A new middle Miocene pliopithecid from
833 Sant Quirze, northern Spain. J. Hum. Evol. 42, 371–377.
834 Harrison, T., Ji, X., Su, D., 2002b. On the systematic status of the late Neogene hominoids
835 from Yunnan Province, China. J. Hum. Evol. 43, 207–227.
836 Harrison, T., Zhang, Y., Wei, G., Sun, C., Wang, Y., Liu, J., Tong, H., Huang, B., Xu, F.,
837 2020. A new genus of pliopithecoid from the late Early Miocene of China and its
838 implications for understanding the paleozoogeography of the Pliopithecoidea. J. Hum.
839 Evol. 145, 102838.
840 Heizmann, E.P.J., Begun, D.R., 2001. The oldest Eurasian hominoid. J. Hum. Evol. 41, 463–
841 481.
842 Kappelman, J., Richmond, B.G., Seiffert, E.R., Maga, A.M., Ryan, T.M., 2003. Hominoidea
843 (Primates). In: Fortelius, M., Kappelman, J., Sen, S., Bernor, R.L. (Eds.), Geology and
844 Paleontology of the Miocene Sinap Formation, Turkey. Columbia University Press, New
845 York, pp. 90–124.
846 Kaup, J.J., 1861. Beiträge zur näheren Kenntniss der urweltlichen Säugethiere. Fuenftes Heft.
847 Eduard Zernin, Darmstadt.
848 Kelley, J., 1997. Paleobiological and phylogenetic significance of life history in Miocene
849 hominoids. In: Begun, D.R., Ward, C.V., Rose, M.D. (Eds.), Function, Phylogeny and
850 Fossils: Miocene Hominoid Evolution and Adaptation. Plenum Press, New York, pp. 173–
851 208.
852 Köhler, M., Alba, D.M., Moyà-Solà, S., MacLatchy, L., 2002. Taxonomic affinities of the
853 Eppelsheim femur. Am. J. Phys. Anthropol. 119, 297–304.
854 Kordos, L., Begun, D.R., 1999. Femora of *Anapithecus* from Rudabánya. Am. J. Phys.

855 Anthropol. 108 (S28), 173.
856 Kordos, L., Begun, D.R., 2001. Primates from Rudabánya: allocation of specimens to
857 individuals, sex and age categories. J. Hum. Evol. 40, 17–39.
858 Larson, S.G., 1998. Parallel evolution in the hominoid trunk and forelimb. Evol. Anthropol. 6,
859 87–99.
860 Le Gros Clark, W.E., Thomas, D.P., 1951. Associated jaws and limb bones of *Limnopithecus*
861 *macinnesi*. Foss. Mamm. Afr. 3, 1–27.
862 Leakey, R.E., Leakey, M.G., 1986. A second new hominoid from Kenya. Nature 324, 143–
863 146.
864 Leakey, R.E., Leakey, M.G., Walker, A.C., 1988. Morphology of *Turkanapithecus*
865 *kalakolensis* from Kenya. Am. J. Phys. Anthropol. 76, 277–288
866 Lin, Y., Wang, S., Guo, Z., Zhang, L., 1987. The first discovery of the radius of *Sivapithecus*
867 *lufengensis* in China. Geol. Rev. 33, 1–4.
868 Marigó, J., Susanna, I., Minwer-Barakat, R., Madurell-Malapeira, J., Moyà-Solà, S.,
869 Casanovas-Vilar, I., Robles, J.M., Alba, D.M., 2014. The primate fossil record in the
870 Iberian Peninsula. J. Iber. Geol. 40, 179–211.
871 McCrossin, L.M., Benefit, B.R., Giteu, S.N., Palmer, A.K., Blue, K.T., 1998. Fossil evidence
872 for the origins of terrestriality among Old World higher primates. In: Strasser, E., Fleagle,
873 J., Rosenberger, A., McHenry, H. (Eds.), Primate Locomotion: Recent Advances. Plenum
874 Press, New York, pp. 353–396.
875 McNulty, K.P., Begun, D.R., Kelley, J., Manthi, F.K., Mbua, E.N., 2015. A systematic
876 revision of *Proconsul* with the description of a new genus of early Miocene hominoid. J.
877 Hum. Evol. 84, 42–61.
878 Meldrum, D.J., Pan, Y., 1988. Manual proximal phalanx of *Laccopithecus robustus* from the
879 Latest Miocene site of Lufeng. J. Hum. Evol. 17, 719–731.
880 Mitteroecker, P., Bookstein, F., 2011. Linear discrimination, ordination, and the visualization

881 of selection gradients in modern morphometrics. Evol. Biol. 38, 100–114.
882 Morbeck, M.E., 1975. *Dryopithecus africanus* forelimb. J. Hum. Evol. 4, 39–46.
883 Morbeck, M.E., 1976. Problems in reconstruction of fossil anatomy and locomotor behavior:
884 the *Dryopithecus* elbow complex. J. Hum. Evol. 5, 223–233.
885 Morbeck, M.E., 1983. Miocene hominoid discoveries from Rudabánya. Implications from the
886 postcranial skeleton. In: Ciochon, R.L., Corruccini, R.S. (Eds.), New Interpretations of
887 Ape and Human Ancestry. Plenum Publishing Corporation, New York, pp. 369–404.
888 Moyà-Solà, S., Köhler, M., 1996. A *Dryopithecus* skeleton and the origins of great-ape
889 locomotion. Nature 379, 156–159.
890 Moyà-Solà, S., Köhler, M., Alba, D.M., 2001. *Egarapithecus narcisoi*, a new genus of
891 Pliopithecidae (Primates, Catarrhini) from the Late Miocene of Spain. Am. J. Phys.
892 Anthropol. 114, 312–324.
893 Moyà-Solà, S., Köhler, M., Rook, L., 2005. The *Oreopithecus* thumb: a strange case in
894 hominoid evolution. J. Hum. Evol. 49, 395–404.
895 Napier, J.R., Davis, P.R., 1959. The fore-limb skeleton and associated remains of *Proconsul*
896 *africanus*. Foss. Mamm. Afr. 16, 1–69.
897 Nengo, I., Tafforeau, P., Gilbert, C.C., Fleagle, J.G., Miller, E.R., Feibel, C., Fox, D.L.,
898 Feinberg, J., Pugh, K.D., Berruyer, C., Mana, S., Engle, Z., Spoor, F., 2017. New infant
899 cranium from the African Miocene sheds light on ape evolution. Nature 548, 169–174.
900 O'Higgins, P., 2000. The study of morphological variation in the hominid fossil record:
901 biology, landmarks and geometry. J. Anat. 197, 103–120.
902 Oksanen, J., Blanchet, F.G., Friendly, M., Kindt, R., Legendre, P., McGlinn, D., Minchin,
903 P.R., O'Hara, R. B., Simpson, G.L., Solymos, P., Stevens, M.H.H., Szoecs, E., Wagner. H.,
904 2020. Package "Vegan": Community Ecology Package. R package version 2.5-7.
905 https://CRAN.R-project.org/package=vegan.
906 Pagel, M., 1999. Inferring the historical patterns of biological evolution. Nature 401, 877–

884.

Patel, B.A., 2005. The hominoid proximal radius: re-interpreting locomotor behaviors in early hominins. J. Hum. Evol. 48, 415–432.

Peppe, D.J., McNulty, K., Cote, S.M., Harcourt-Smith, W.E.H., Dunsworth, H.M., Van Couvering, J.A., 2009. Stratigraphic interpretation of the Kulu Formation (Early Miocene, Rusinga Island, Kenya) and its implications for primate evolution. J. Hum. Evol. 56, 447–461.

Pohlig, H., 1895. *Paidopithex rhenanus*, n.g.n.s., le singe anthropomorphe du Pliocene rhenan. Bull. Soc. Belge Géol. 9, 149–151.

R Core Team, 2019. R: A language and environment for statistical computing. R Foundation for Statistical Computing, Vienna.

Rein, T.R., Harrison, T., Zollikofer, C.P.E., 2011. Skeletal correlates of quadrupedalism and climbing in the anthropoid forelimb: implications for inferring locomotion in Miocene catarrhines. J. Hum. Evol. 61, 564–574.

Rein, T.R., Harvati, K., Harrison, T., 2015. Inferring use of forelimb suspensory locomotion by extinct primate species via shape exploration of the ulna. J. Hum. Evol. 78, 70–79.

Revell, L.J., 2012. Phytools: an R package for phylogenetic comparative biology (and other things). Methods Ecol. Evol. 3, 217–223.

Roos, C., Kothe, M., Alba, D.M., Delson, E., Zinner, D., 2019. The radiation of macaques out of Africa: Evidence from mitogenome divergence times and the fossil record. J. Hum. Evol. 133, 114–132.

Rose, M.D., 1983. Miocene hominoid postcranial morphology monkey-like, ape-like, neither, or both? In: Ciochon, R.L., Corruccini, R.S. (Eds.), New Interpretations of Ape and Human Ancestry. Plenum Publishing Corporation, New York, pp. 405–417.

Rose, M.D., 1988. Another look at the anthropoid elbow. J. Hum. Evol. 17, 193–224.

Rose M.D., 1993b. Functional anatomy of the elbow and forearm in primates. In: Gebo, D.L.

(Ed.), Postcranial Adaptation in Nonhuman Primates. Northern Illinois University, DeKalb, pp. 70–95.

Rose, M.D., 1993a. Locomotor anatomy of Miocene hominoids. In: Gebo, D.L. (Ed.), Postcranial Adaptation in Nonhuman Primates. Northern Illinois University Press, DeKalb, pp. 252–272.

Rose, M.D., 1994. Quadrupedalism in some Miocene catarrhines. J. Hum. Evol. 26, 387–411.

Rose, M.D., 1997. Functional and phylogenetic features of the forelimb in Miocene hominoids. In: Begun, D.R., Ward, C.V., Rose, M.D. (Eds.), Function, Phylogeny and Fossils: Miocene Hominoid Evolution and Adaptation. Plenum Press, New York, pp. 79–100.

Rose, M.D., Leakey, M.G., Leakey, R.E.F., Walker, A.C., 1992. Postcranial specimens of *Simiolus enjiessi* and other primitive catarrhines from the early Miocene of Lake Turkana, Kenya. J. Hum. Evol. 22, 171–237.

Rossie, J.B., Gutierrez, M., Goble, E., 2012. Fossil forelimbs of *Simiolus* from Moruorot, Kenya. Am. J. Phys. Anthropol. 147 (S54), 252.

Rossie, J.B., MacLatchy, L., 2006. A new pliopithecoid genus from the early Miocene of Uganda. J. Hum. Evol. 50, 568–586.

Ruff, C.B., 2002. Long bone articular and diaphyseal structure in Old World monkeys and apes. I: Locomotor effects. Am. J. Phys. Anthropol. 119, 305–342.

Ruff, C.B., 2003. Long bone articular and diaphyseal structure in Old World monkeys and apes. II: Estimation of body mass. Am. J. Phys. Anthropol. 120, 16–37.

Sankhyan, A.R., Kelley, J., Harrison, T., 2017. A highly derived pliopithecoid from the Late Miocene of Haritalyangar, India. J. Hum. Evol. 105, 1–12.

Sarmiento, E.E., 1987. The phylogenetic position of *Oreopithecus* and its significance in the origin of the Hominoidea. Am. Mus. Nov. 2881, 1–44.

Sarmiento, E.E., 1988. Anatomy of the hominoid wrist joint: its evolutionary and functional

959 implications. Int. J. Primatol. 9, 281–345.
960 Sarmiento, E.E., 1995. Cautious climbing and folivory: a model of hominoid differentiation.
961 Hum. Evol. 10, 289–321.
962 Sarmiento E.E., Stiner, E., Mowbray, K., 2002. Morphology-based systematics (MBS) and
963 problems with fossil hominoid and hominid systematics. Anat. Rec. 269, 50–66.
964 Schlager, S., 2017. Morpho and Rvcg – shape analysis in R: R-packages for geometric
965 morphometrics, shape analysis and surface manipulations. In: Zheng, G., Li, S., Székely,
966 G. (Eds.), Statistical Shape and Deformation Analysis. Methods, Implementation and
967 Applications. Academic Press, London, pp. 217–256.
968 Senut, B., 1989. Le Coude des Primates Hominoïdes. Anatomie, Fonction, Taxonomie,
969 Évolution. Éditions du Centre National de la Recerche Scientifique, Paris.
970 Senut, B., 2012. Les restes post-crâniens des Pliopithecidae (Primates) de Sansan. Mém. Mus.
971 Hist. Nat. Paris 203, 535–558.
972 Shearer, B.M., Cooke, S.B., Halenar, L.B., Reber, S.L., Plummer, J.E., Delson, E., Tallman,
973 M., 2017. Evaluating causes of error in landmark-based data collection using scanners.
974 PLoS One 12, e0187452.
975 Sherwood, R.J., Ward, R.J., Hill, A., Duren, D.L., Brown, B., Downs, W., 2002. Preliminary
976 description of the *Equatorius africanus* partial skeleton KNM-TH 28860 from
977 Kipsaramon, Tugen Hills, Baringo District, Kenya. J. Hum. Evol. 42, 63–73.
978 Sidlauskas, B., 2008. Continuous and arrested morphological diversification in sister clades of
979 characiform fishes: a phylomorphospace approach. Evolution 62, 3135–3156.
980 Smith, R.J., 1993. Bias in equations used to estimate fossil primate body mass. J. Hum. Evol.
981 25, 31–41.
982 Sukselainen, L., Fortelius, M., Harrison, T., 2015. Co-occurrence of pliopithecoid and
983 hominoid primates in the fossil record: An ecometric analysis. J. Hum. Evol. 84, 25–41.

984 Takahashi, L., K., 1990. Morphological basis of arm-swinging: multivariate analyses of the
985 forelimbs of *Hylobates* and *Ateles*. Folia Primatol. 54, 70–85.
986 Tallman, M., 2010. Postcranial variation in Plio-Pleistocene hominins of Africa. Ph.D.
987 Dissertation, The City University of New York.
988 Tallman, M., 2013. Forelimb to hindlimb shape covariation in extant hominoids and fossil
989 hominins. Anat. Rec. 296, 290–304.
990 Tocheri, M.W., Solhan, C. R., Orr, C. M., Femiani, J., Frohlich, B., Groves, C.P., Harcourt-
991 Smith, W.E., Richmond, B.G., Shoelson, B., Jungers, W.L., 2011. Ecological divergence
992 and medial cuneiform morphology in gorillas. J. Hum. Evol. 60, 171–184.
993 Urciuoli, A., Zanolli, C., Beaudet, A., Pina, M., Almécija, S., Moyà-Solà, S., Alba, D.M.,
994 2021. A comparative analysis of the vestibular apparatus in *Epipliopithecus*
995 *vindobonensis*: Phylogenetic implications. J. Hum. Evol. 151, 102930.
996 van der Meulen, A.J., García-Paredes, I., Álvarez-Sierra, M.Á., van den Hoek Ostende, L.W.,
997 Hordijk, K., Oliver, A., López-Guerrero, P., Hernández-Ballarín, V., Peláez-
998 Campomanes, P., 2011. Biostratigraphy or biochronology? Lessons from the Early and
999 Middle Miocene small Mammal Events in Europe. Geobios 44, 309–321.
1000 Walker, A.C., Pickford, M., 1983. New postcranial fossils of *Proconsul africanus* and
1001 *Proconsul nyanzae*. In: Ciochon, R.L., Corruccini, R.S. (Eds.), New Interpretations of Ape
1002 and Human Ancestry. Plenum Press, New York, pp. 325–351.
1003 Ward, C.V., 1993. Torso morphology and locomotion in *Proconsul nyanzae*. Am. J. Phys.
1004 Anthropol. 92, 291–328.
1005 Ward, C.V., 1998. *Afropithecus*, *Proconsul*, and the primitive hominoid skeleton. In: Strasser,
1006 E., Fleagle, J., Rosenberger, A., McHenry, H. (Eds.), Primate Locomotion: Recent
1007 Advances. Plenum Press, New York, pp. 337–352.
1008 Ward, C.V., 2015. Postcranial and locomotor adaptations of hominoids. In: Henke, W.,
1009 Tattersall, I. (Eds.), Handbook of Paleoanthropology, 2nd ed. Springer, Heidelberg, pp.

1363–1386.

Ward, C.V., Walker, A., Teaford, M.F., Odhiambo, L., 1993. Partial skeleton of *Proconsul nyanzae* from Mfangano Island, Kenya. Am. J. Phys. Anthropol. 90, 77–111.

Ward, S., Brown, B., Hill, A., Kelley, J., Downs, W., 1999. *Equatorius*: a new hominoid genus from the middle Miocene of Kenya. Science 285, 1382–1386.

Wiley, D.F., Amenta, N., Alcantara, D.A., Ghosh, D., Kil, Y.J., Delson, E., Harcourt-Smith, W., Rohlf, F.J., St John, K., Hamann, B., 2005. Evolutionary morphing. In: Silva, T.C., Gorller, E., Rushmeier, H. (Eds.), VIS 05 IEEE Visualization. IEEE, Minneapolis, pp. 431–438.

Youlatos, D., 1993. Passages within a discontinuous canopy: Bridging in the red howler monkey (*Alouatta seniculus*). Folia Primatol. 66, 144–147.

Zapfe, H., 1958. The skeleton of *Pliopithecus (Epipliopithecus) vindobonensis* Zapfe and Hürzeler. Am. J. Phys. Anthropol. 16, 441–457.

Zapfe, H., 1961. Die Primatenfunde aus der miozänen Spaltenfüllung von Neudorf an der March (Děvínská Nová Ves), Tschechoslowakei. Schweizer. Palaeontol. Abh. 78, 1–293.

Zapfe, H., Hürzeler, J., 1957. Die Fauna der miozänen Spaltenfüllung von Neudorf an der March (ČSR.). Primates. Sitz.-ber. Österr. Akad. Wiss. Math.-natur. Kl. Abt. I 166, 113–123.

Figure captions

Figure 1. Right proximal radius (IPS66267) of *Barberapithecus huerzeleri* from Castell de Barberà, in anterior (a), lateral (b), posterior (c), medial (d) and proximal (e) views. See 3D model in SOM File S1.

1035 **Figure 2.** Landmark protocol illustrated on 3D model renderings of the *Barberapithecus*
1036 *huerzeleri* left proximal radial fragment (IPS66267, mirrored), in superior (a), anterior (b),
1037 lateral (c), medial (d) and posterior (e) views. Landmarks (L) are described in Table 2.
1038
1039 **Figure 3.** The right proximal radius (IPS66267) of *Barberapithecus huerzeleri* from Castell
1040 de Barberà, in anterior (a) and proximal (b) views, compared with selected fossil and extant
1041 catarrhines, including: *Simiolus enjiessi* KNM-MO 63 from Moruorot (right), in anterior (c)
1042 and proximal (d) views; *Epipliopithecus vindobonensis* from Děvínská Nová Ves (individual
1043 I, right), in anterior (e) and proximal (f) views; and *Hylobates* sp. (right), in anterior (g) and
1044 proximal (h) views. Artwork by Marta Palmero.
1045
1046 **Figure 4.** Results of the between-group principal component analysis as depicted by a
1047 bivariate plot of bgPC2 vs. bgPC1. Groups distinguished a priori are denoted with different
1048 colors: violet = hominids; green = hylobatids; dark yellow = cercopithecines; blue =
1049 colobines; pink = platyrrhines. Fossil specimens (scores projected a posteriori) are denoted by
1050 stars. Abbreviation: bgPC = between-group principal component.
1051
1052 **Figure 5.** Phylomorphospace of proximal radius shape in anthropoid primates. The
1053 phylogenetic tree on the left is projected onto the tangent space defined by the bgPCs as
1054 shown in Figure 4. Ancestral states inferred for the LCAs of main anthropoid clades based on
1055 maximum likelihood (assuming Brownian motion) are denoted by colored pentagons. The
1056 branches are colored according to the phylogeny of the groups in both the phylogenetic tree
1057 and the phylomorphospace. The fossils are denoted with colored stars as shown in Figure 4
1058 (except for *Simiolus*, which is an average of the two specimens analyzed). The inset to the
1059 right is a close-up of the dashed area in the phylomorphospace. Abbreviations: bgPC =
1060 between-group principal component; LCA = last common ancestor.

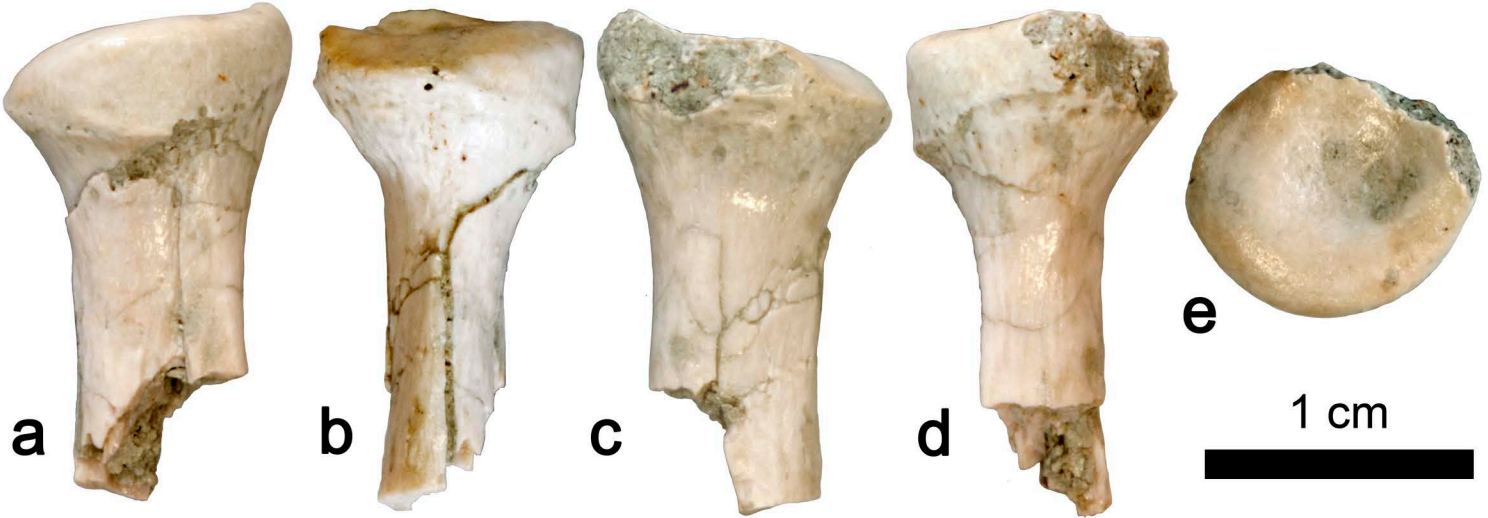
a
b
c
d
e
1 cm

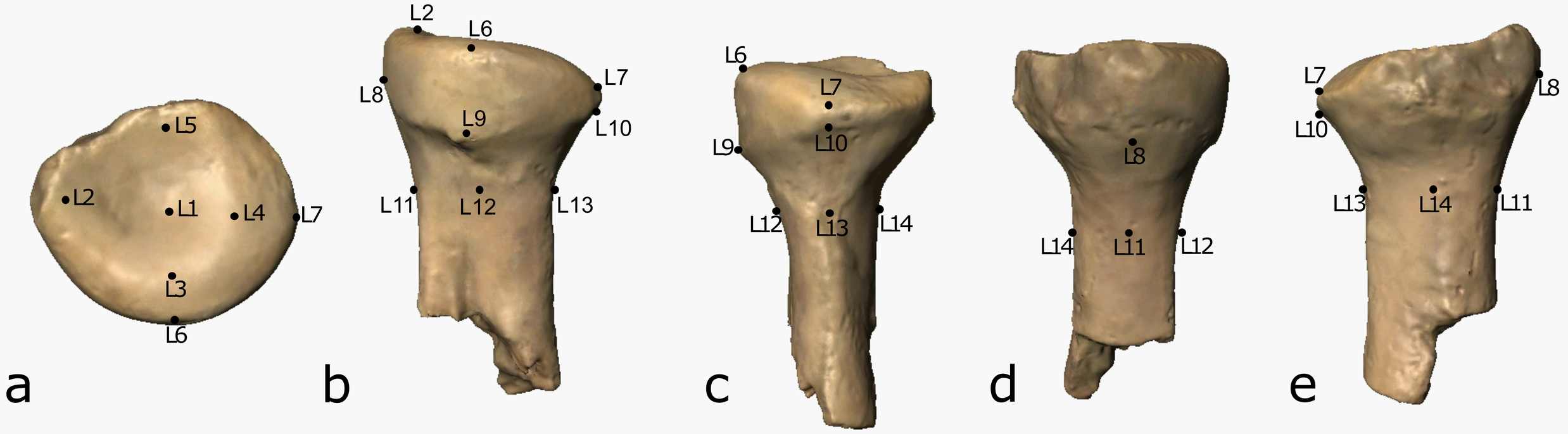
L5
L2
L1
L4
L7
L3
L6
a
L2
L6
L8
L7
L9
L10
L11
L12
L13
b
L6
L7
L9
L10
L12
L13
L14
c
L8
L14
L11
L12
d
L7
L8
L10
L13
L14
L11
e

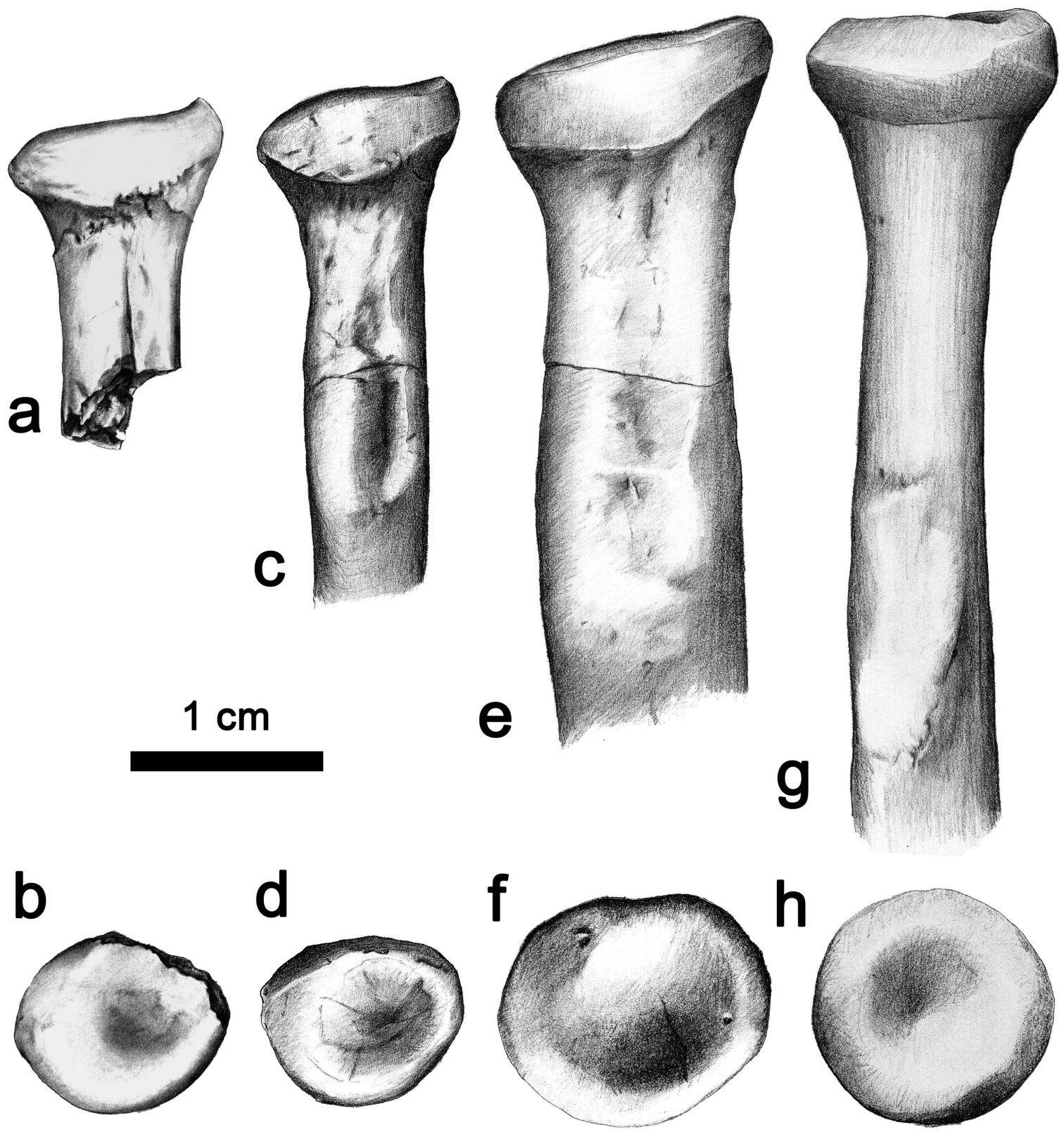
a
c
e
g
1 cm
b
d
f
h

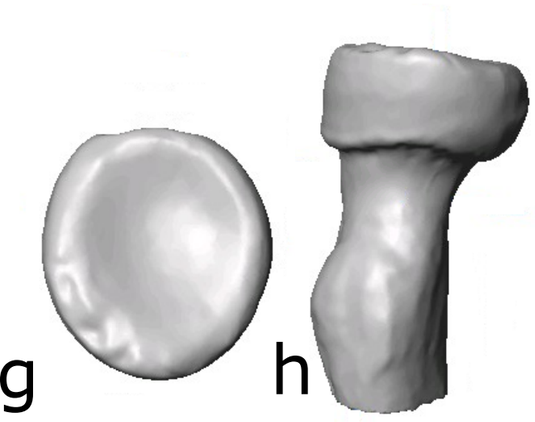
g
h

0.1
0.0
−0.1
−0.2
bgPC2 (18.7% of variance)
−0.1
0.0
0.1
bgPC1 (69% of variance)
Gorilla
Pongo
Pan
Homo
Nomascus
Hylobates
Symphalangus
Hoolock
Mandrillus
Macaca
Papio
Colobus
Nasalis
Alouatta
Cebus
Ateles
Lagothrix
Ekembo heseloni
Simiolus enjiessi (KNM-MO 63)
Simiolus enjiessi (KNM-MO 17022B)
Epipliopithecus vindobonensis
Dendropithecus macinnesi
Barberapithecus huerzeleri

e
f

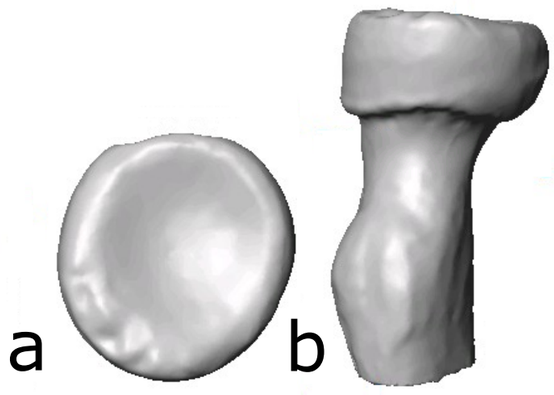
a
b

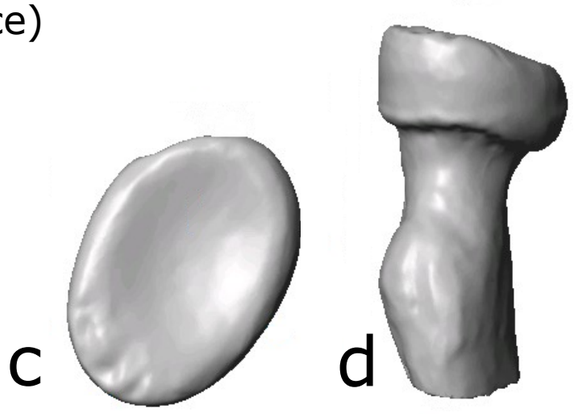
c
d

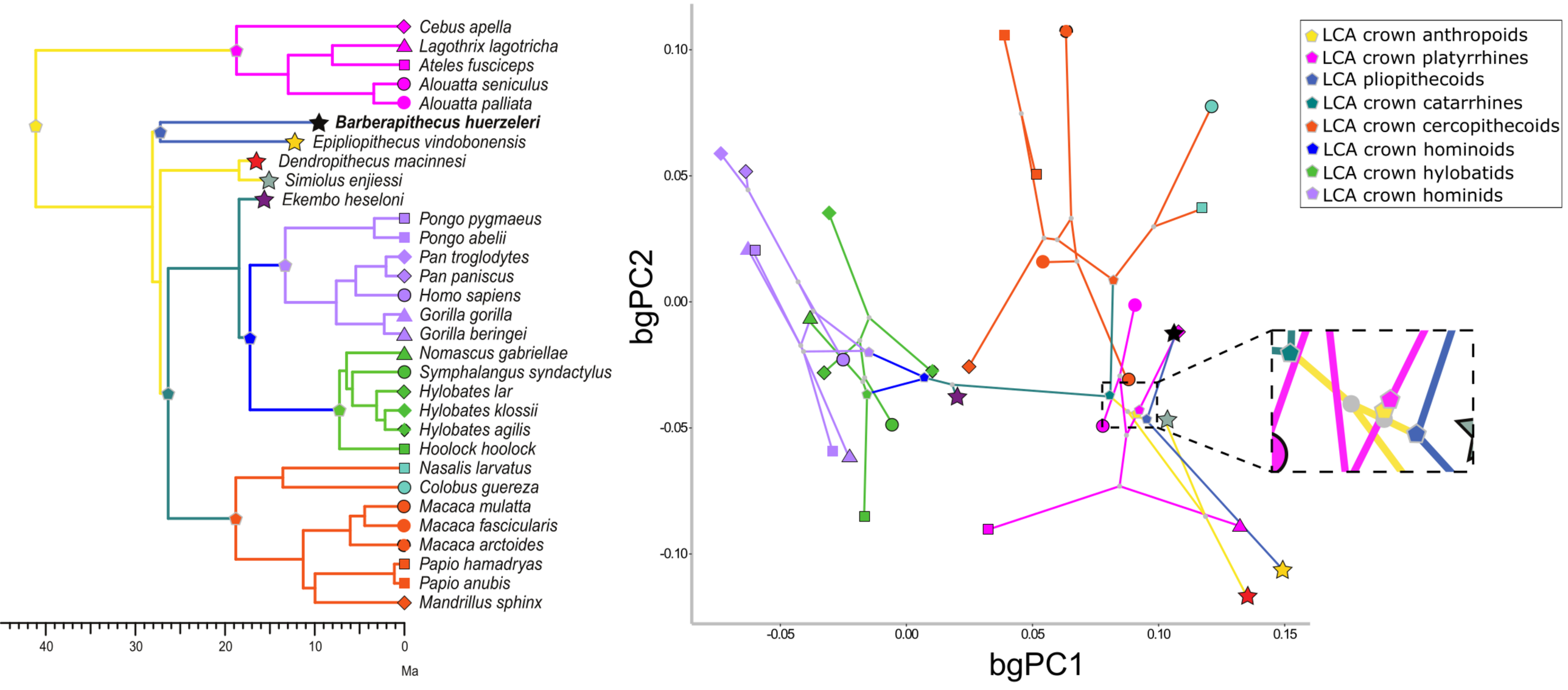
Cebus apella
Lagothrix lagotricha
Ateles fusciceps
Alouatta seniculus
Alouatta palliata
Barberapithecus huerzeleri
Epipliopithecus vindobonensis
Dendropithecus macinnesi
Simiolus enjiessi
Ekembo heseloni
Pongo pygmaeus
Pongo abelii
Pan troglodytes
Pan paniscus
Homo sapiens
Gorilla gorilla
Gorilla beringei
Nomascus gabriellae
Symphalangus syndactylus
Hylobates lar
Hylobates klossii
Hylobates agilis
Hoolock hoolock
Nasalis larvatus
Colobus guereza
Macaca mulatta
Macaca fascicularis
Macaca arctoides
Papio hamadryas
Papio anubis
Mandrillus sphinx
40
30
20
10
0
Ma
LCA crown anthropoids
LCA crown platyrrhines
LCA pliopithecoids
LCA crown catarrhines
LCA crown cercopithecoids
LCA crown hominoids
LCA crown hylobatids
LCA crown hominids
0.10
0.05
0.00
-0.05
-0.10
bgPC2
-0.05
0.00
0.05
0.10
0.15
bgPC1

Table 1

Summary of the extant primate sample used in this study.[a]

Taxon	*n*	Sex (M/F/?)	Side (L/R)	Repositories
Gorilla	15	7/5/3	11/4	AMNH, USNM, RMCA, CMNH, PCM, MS
Pan	20	10/8/2	16/4	AMNH, USNM, RMCA, TC MPI-EVA, SBU, MS
Homo	5	2/2/1	5/0	AMNH, USNM, MS
Pongo	19	6/7/6	16/3	AMNH, USNM, ZMB, ZMS, MS
Hylobates	4	2/2/0	3/1	AMNH, USNM
Nomascus	1	0/1/0	1/0	AMNH
Hoolock	2	1/1/0	0/2	AMNH
Symphalangus	8	1/2/5	6/2	AMNH, USNM, ZMB, MS
Macaca	8	2/2/4	6/2	AMNH, USNM, ZMB, MS
Papio	6	2/2/2	5/1	AMNH, USNM, ZMB
Mandrillus	2	2/0/0	0/2	MS
Colobus	5	2/3/0	5/0	AMNH, USNM
Nasalis	3	2/1/0	3/0	AMNH, USNM
Cebus	6	5/1/0	2/4	AMNH, USNM
Ateles	6	2/2/2	3/3	USNM, ZMB
Lagothrix	1	0/0/1	0/1	MS
Alouatta	6	3/2/1	5/1	AMNH, USNM, ZMB, ZMS

Abbreviations: M = male; F = female; ? = unknown sex; L = left; R = right; AMNH = American Museum of Natural History, New York, USA; USNM = Smithsonian National Museum of Natural History, Washington D.C., USA; RMCA = Royal Museum for Central Africa, Tervuren, Belgium; CMNH = Cleveland Museum of Natural History, Cleveland, USA; PCM = Powell-Cotton Museum, Birchington, UK; TC MPI-EVA = Tai Forest Collection, Max Planck Institute for Evolutionary Anthropology, Leipzig, Germany; ZMB = Museum für Naturkunde – Leibniz Institute for Evolution

and Biodiversity Science, Berlin, Germany; ZMS = Zoologische Staatssammlung Munchen, Munich, Germany; SBU = Stony Brook University; MS = MorphoSource.

[a] See SOM Table S1 for the collection numbers of all the specimens included.

Table 2

Landmark protocol used in this study.[a]

Landmark No.	Description
Fovea capitis:	
L1	Deepest point of the fovea capitis
L2	Most medial point on fovea capitis outline
L3	Most anterior point on fovea capitis outline
L4	Most lateral point on fovea capitis outline
L5	Most posterior point on fovea capitis outline
Radial head:	
L6	Most anterior point on radial head outline
L7	Most lateral point on radial head outline
L8	Most medial point on distal articular expansion of the radial head
L9	Most anterior point on distal articular expansion of the radial head
L10	Most lateral point on distal articular expansion of the radial head
Radial neck:	
L11	Most medial point on radial neck
L12	Most anterior point on radial neck
L13	Most lateral point on radial neck
L14	Most posterior point on radial neck

[a] All landmarks used are type II/III (sensu Bookstein et al., 1999; O'Higgins, 2000).

Table 3

Body mass estimates for *Barberapithecus huerzeleri*.[a]

Molar	Catalog No.	MD	BL	A	BM	95% CI
M^1	IPS1724c	5.3	6.5	34.45	5.20	4.22, 6.17
M^2	IPS1724d,e	5.6	7	39.20	5.74	4.79, 6.70
M_1	IPS1724m	5.7	4.6	26.22	4.73	4.02, 5.44
M_2	IPS1724n	6.4	5.1	32.64	5.40	4.62, 6.17
Average[b]	IPS1724	—	—	—	5.27	4.02, 6.70
Radius	Catalog No.	RHML	RHAP	RHSA	BM	95% CI
Radial head	IPS66267	11.27	9.61	85.02	4.85	4.40, 5.30

Abbreviations: MD = mesiodistal length (mm); BL = buccolingual breadth (mm); A = occlusal area (mm^2), computed as MD × BL; BM = estimated body mass (kg); RHML = radial head mediolateral breadth (mm); RHAP = radial head anteroposterior breadth (mm); RHSA = radial head surface area (mm^2), computed as 0.785 × RHML × RHAP.

[a] Dental BM estimates were derived using the anthropoid equations of Egi et al. (2004), while the postcranial estimate was derived using Ruff's (2003: Table 7) 'total sample' (hominoids + cercopithecoids) equation for the proximal radius. The CIs were computed based on the standard error of estimate reported by these authors and an inverse Student's t distribution with degrees of freedom = $n - 2$ (Ruff, 2003) or effective n (Egi et al., 2004).

[b] Average BM is the mean of the estimates derived for the four molars of IPS1724 (holotype), but average CI is based on the minimum and maximum values for all these molars considered together.

Supplementary Online Material (SOM):

A proximal radius of *Barberapithecus huerzeleri* from Castell de Barberà: Implications for locomotor diversity among pliopithecoids

Julia Arias-Martorell [a,b,*], Sergio Almécija [c,d,a], Alessandro Urciuoli [a], Masato Nakatsukasa[e], Salvador Moyà-Solà [a,f,g], David M. Alba[a,*]

[a] *Institut Català de Paleontologia Miquel Crusafont, Universitat Autònoma de Barcelona, Edifici ICTA-ICP, c/ Columnes s/n, Campus de la UAB, 08193 Cerdanyola del Vallès, Barcelona, Spain*

[b] *School of Anthropology and Conservation, Marlowe Building University of Kent, Canterbury, UK CT2 7NR, UK*

[c] *Division of Anthropology, American Museum of Natural History, Central Park West at 79th Street, New York, NY 10024, USA*

[d] *New York Consortium in Evolutionary Primatology, New York, NY 10024, USA*

[e] *Laboratory of Physical Anthropology, Graduate School of Science, Kyoto University, 606-8502 Kyoto, Japan;*

[f] *Institució Catalana de Recerca i Estudis Avançats (ICREA), Passeig de Lluís Companys 23, 08010 Barcelona, Spain*

[g] *Unitat d'Antropologia Biològica (Departament de Biologia Animal, Biologia Vegetal i Ecologia), Universitat Autònoma de Barcelona, 08193 Cerdanyola del Vallès, Barcelona, Spain*

[*]Corresponding authors.

E-mail addresses: julia.arias@icp.cat (J. Arias-Martorell); david.alba@icp.cat (D.M. Alba).

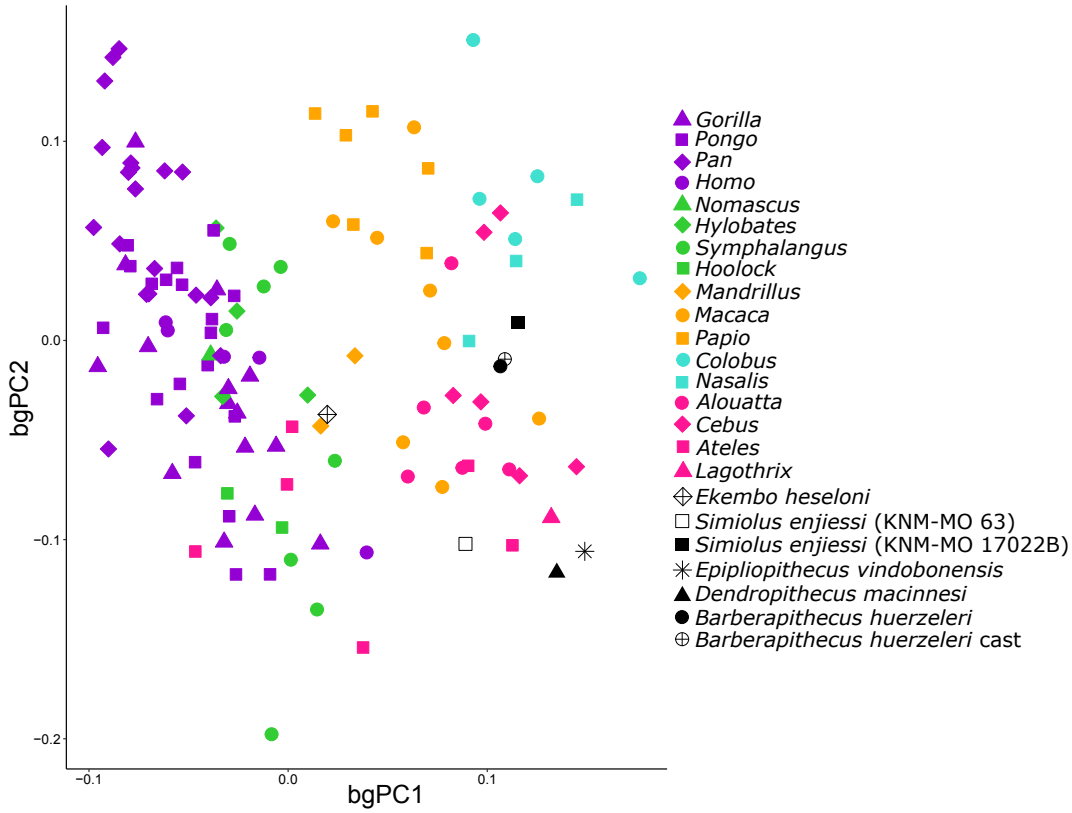

SOM Figure S1. Results of the between-group principal component analysis depicted as a bivariate plot of bgPC2 vs. bgPC1 of proximal radius shape among extant anthropoid primates, the fossils included in the analysis and the high-resolution cast of *Barberapithecus* showing little deviation from the original specimen. Abbreviation: bgPC = between-group principal component.

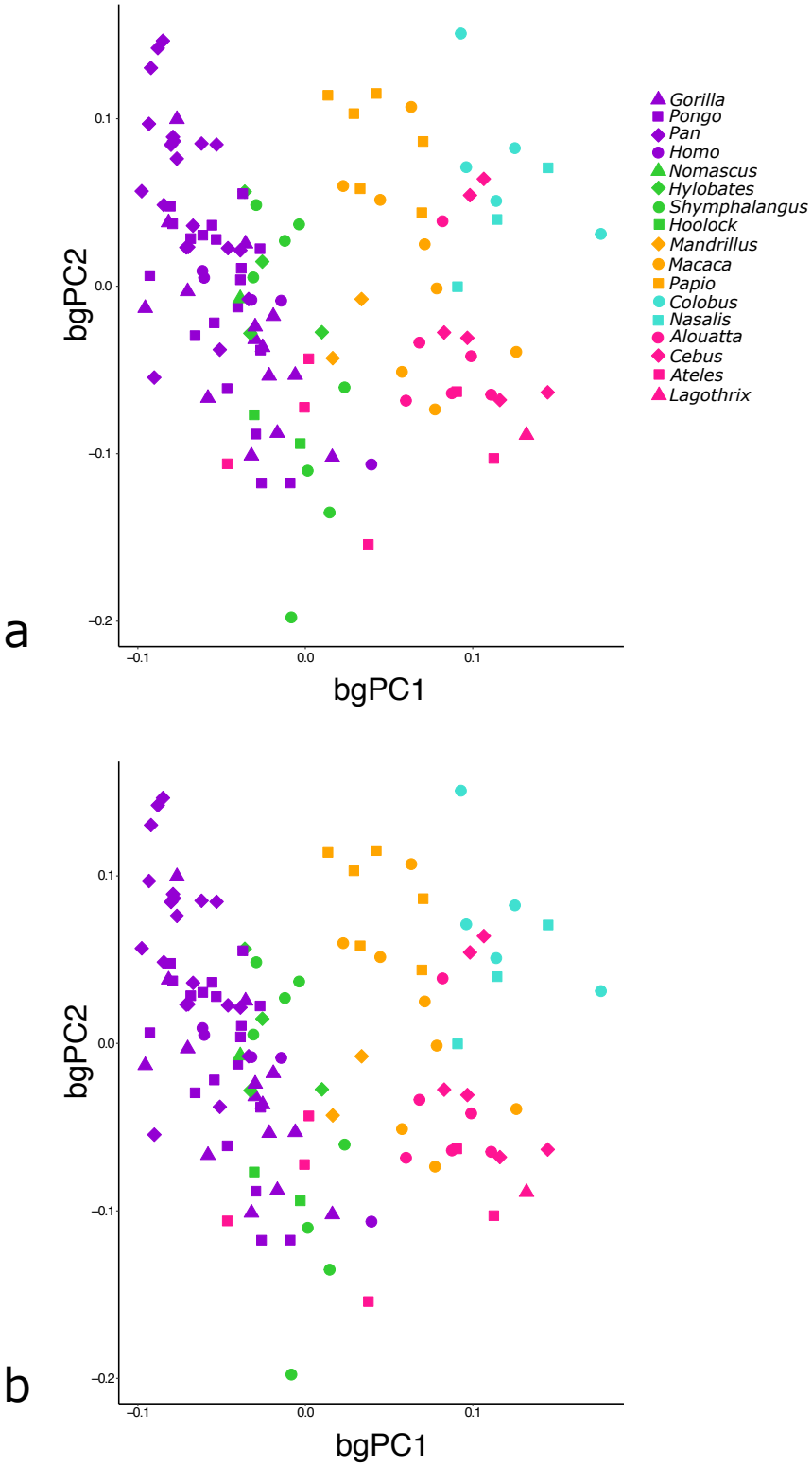

SOM Figure S2. Results of the between-group principal component analysis of proximal radius shape among extant anthropoid primates as depicted by bivariate plots of bgPC2 vs. bgPC1 before (a) and after (b) cross-validation. Abbreviation: bgPC = between-group principal component.

SOM Table S1

Details of the extant primate sample used in the study. Media and identifier (when available) are listed for specimens downloaded from Morphosource.org.

Species	Catalog No.	Sex	Side	Source	Media	Identifier	Scanner
Alouatta palliata aequatorialis	USNM 338107	M	L	USNM	—	—	NextEngine
Alouatta palliata palliata	USNM 282798	F	L	USNM	—	—	NextEngine
Alouatta seniculus	AMNH 42316	F	L	AMNH	—	—	NextEngine
Alouatta seniculus	AMNH 23333	M	L	AMNH	—	—	NextEngine
Alouatta sp	ZMB 35764	M	L	ZMB	—	—	µCT (BIR ACTIS)
Alouatta sp	ZMS 1973-0330	?	R	ZMS	—	—	µCT (BIR ACTIS)
Ateles fusciceps robustus	USNM 338111	F	L	USNM	—	—	NextEngine
Ateles fusciceps robustus	USNM 338112	M	L	USNM	—	—	NextEngine
Ateles sp	ZMB 45255	F	R	ZMB	—	—	µCT (BIR ACTIS)
Ateles sp	ZMB 44814	M	R	ZMB	—	—	µCT (BIR ACTIS)
Ateles sp	ZMB 38734	?	R	ZMB	—	—	µCT (BIR ACTIS)
Ateles sp	ZMB 44079	?	L	ZMB	—	—	µCT (BIR ACTIS)
Cebus apella apella	USNM 361020	M	L	USNM	—	—	NextEngine
Cebus apella	USNM 397940	F	R	USNM	—	—	NextEngine
Cebus apella	AMNH 133606	M	L	AMNH	—	—	NextEngine
Cebus apella paraguanayanus	AMNH 133631	M	R	MS	M12099-19605	urn:catalog:AMNH:Mammals:M-133631	—
Cebus apella paraguayanus	AMNH 133623	M	R	MS	M12095-19594	urn:catalog:AMNH:Mammals:M-133623	—
Cebus apella paraguayanus	AMNH 133628	M	R	MS	M12093-19588	urn:catalog:AMNH:Mammals:M-133628	—
Colobus guereza	AMNH 52223	F	L	AMNH	—	—	NextEngine
Colobus guereza	AMNH 52241	F	L	AMNH	—	—	NextEngine
Colobus guereza kikuyuensis	USNM 452621	M	L	USNM	—	—	NextEngine
Colobus guereza	AMNH 52248	M	L	AMNH	—	—	NextEngine
Colobus guereza	USNM 452632	F	L	USNM	—	—	NextEngine
Gorilla beringei beringei	AMNH 54091	F	L	AMNH	—	—	NextEngine

Gorilla beringei beringei	RMCA 2263	F	L	RMCA	—	—	NextEngine
Gorilla beringei beringei	USNM 395636	M	L	USNM	—	—	NextEngine
Gorilla beringei beringei	USNM 396934	?	L	Morphosource	M56720-102006	http://n2t.net/ark:/65665/313444cf4-f1e7-4bbc-ba69-039e4d4557e4	—
Gorilla beringei beringei	USNM 396937	?	L	Morphosource	M57009-102295	http://n2t.net/ark:/65665/32f41b8f5-9a15-4f88-af7e-8218ebf0b616	—
Gorilla beringei beringei	USNM 397351	?	L	Morphosource	M56268-101554	http://n2t.net/ark:/65665/3db306794-3c8e-4930-bb20-e514ac62bac6	—
Gorilla beringei graueri	AMNH 202932	M	R	AMNH	—	—	NextEngine
Gorilla beringei graueri	RMCA 8187	M	L	RMCA	—	—	NextEngine
Gorilla beringei	USNM 239883	M	L	USNM	—	—	NextEngine
Gorilla gorilla	USNM 586541	F	R	USNM	—	—	NextEngine
Gorilla gorilla gorilla	AMNH 1673390	F	L	AMNH	—	—	NextEngine
Gorilla gorilla	CMNH 2767	M	L	CMNH	—	—	NextEngine
Gorilla gorilla	USNM 174722	M	R	USNM	—	—	NextEngine
Gorilla gorilla	USNM 176225	M	L	USNM	—	—	NextEngine
Gorilla gorilla	MER 300	F	R	PCM	—	—	µCT (Nikon)
Homo sapiens	AMNH 99-8376	F	L	AMNH	—	—	NextEngine
Homo sapiens	USNM 1512	F	L	USNM	—	—	NextEngine
Homo sapiens	AMNH 20-3501	M	L	AMNH	—	—	NextEngine
Homo sapiens	USNM 942	M	L	USNM	—	—	NextEngine
Homo sapiens	PSU 105-1793	?	L	MS	M45359-82651	—	—
Hoolock hoolock	AMNH 83425	F	R	AMNH	—	—	NextEngine
Hoolock hoolock	AMNH 83420	M	R	AMNH	—	—	NextEngine
Hylobates agilis	AMNH 106575	F	L	AMNH	—	—	NextEngine
Hylobates klossii	AMNH 103344	M	R	AMNH	—	—	NextEngine
Hylobates klossii	AMNH 103347	M	L	AMNH	—	—	NextEngine
Hylobates lar vestitus	NMNH 271047	F	L	USNM	—	—	NextEngine
Lagothrix lagotricha	DU-BAA 90	?	R	MS	M12471-20497	—	—
Macaca arctoides	AMNH 112727	F	L	AMNH	—	—	NextEngine
Macaca fascicularis	USNM 271168	M	R	USNM	—	—	NextEngine
Macaca fascicularis	ZMB 48496	?	L	ZMB	—	—	µCT (BIR ACTIS)

Macaca fascicularis	ZMB 49090	?	L	ZMB	—	—	µCT (BIR ACTIS)
Macaca fascicularis	ZMB 49092	?	L	ZMB	—	—	µCT (BIR ACTIS)
Macaca mulatta	DU-BAA 142	?	R	MS	M12472-20500	—	—
Macaca mulatta	USNM 537241	F	L	USNM	—	—	NextEngine
Macaca mulatta	USNM 537253	M	L	USNM	—	—	NextEngine
Mandrillus sphinx	AMNH 89361	M	R	MS	M10169-14599	urn:catalog:AMNH:Mammals:M-89361	—
Mandrillus sphinx	AMNH 89365	M	R	MS	M10176-14633	urn:catalog:AMNH:Mammals:M-89365	—
Nasalis larvatus	USNM 536050	F	L	USNM	—	—	NextEngine
Nasalis larvatus	AMNH 106275	M	L	AMNH	—	—	NextEngine
Nasalis larvatus	AMNH 198276	M	L	USNM	—	—	NextEngine
Nomascus gabriellae	AMNH 87253	F	L	AMNH	—	—	NextEngine
Pan paniscus	AMNH 86857	F	L	AMNH	—	—	NextEngine
Pan paniscus	RMCA 29045	F	L	RMCA	—	—	NextEngine
Pan paniscus	RMCA 27696	M	R	RMCA	—	—	NextEngine
Pan paniscus	SBU 87-1	M	L	SBU	—	—	NextEngine
Pan troglodytes	USNM 176226	F	L	USNM	—	—	NextEngine
Pan troglodytes	USNM 176229	F	L	USNM	—	—	NextEngine
Pan troglodytes	USNM 176227	M	L	USNM	—	—	NextEngine
Pan troglodytes	USNM 220327	M	L	USNM	—	—	NextEngine
Pan troglodytes	USNM 395820	M	L	USNM	—	—	NextEngine
Pan troglodytes	UNSM 481804	M	R	USNM	—	—	NextEngine
Pan troglodytes schweinfurthii	AMNH 51376	M	R	MS	M10175-14630	urn:catalog:AMNH:Mammals:M-51376	—
Pan troglodytes schweinfurthii	AMNH 51393	M	R	MS	M10242-14814	urn:catalog:AMNH:Mammals:M-51393	—
Pan troglodytes troglodytes	AMNH 54330	M	L	MS	M10240-14808	urn:catalog:AMNH:Mammals:M-54330	—
Pan troglodytes troglodytes	USNM 220064	F	L	USNM	—	—	NextEngine
Pan troglodytes troglodytes	USNM 220062	?	L	MS	M56889-102175	http://n2t.net/ark:/65665/3dcfb7753-f4d7-4334-9b52-6f9f1b9ea03e	—
Pan troglodytes troglodytes	USNM 220063	?	L	MS	M56483-101769	http://n2t.net/ark:/65665/386ed1f25-2f34-459d-91e5-d0111c2e0dc6	—
Pan troglodytes verus	MPI-EVA 11778	F	L	MPI	—	—	µCT (BIR ACTIS)
Pan troglodytes verus	MPI-EVA 13429	F	L	MPI	—	—	µCT (BIR ACTIS)

Pan troglodytes verus	MPI-EVA 15001	F	L	MPI	—	—	µCT (BIR ACTIS)
Pan troglodytes verus	AMNH 89406	M	L	AMNH	—	—	NextEngine
Papio anubis	AMNH 52668	F	L	AMNH	—	—	NextEngine
Papio anubis	AMNH 120388	M	L	AMNH	—	—	NextEngine
Papio anubis neumanni	USNM 384235	F	L	USNM	—	—	NextEngine
Papio anubis neumanni	USNM 384229	M	L	USNM	—	—	NextEngine
Papio hamadryas	ZMB 105450	?	R	ZMB	—	—	µCT (BIR ACTIS)
Papio hamadryas	ZMB 65265	?	L	ZMB	—	—	µCT (BIR ACTIS)
Pongo abelii	USNM 588109	F	L	USNM	—	—	NextEngine
Pongo abelii	UNSM 143588	M	L	USNM	—	—	NextEngine
Pongo abelii	USNM 143587	?	L	MS	M56592-101878	http://n2t.net/ark:/65665/33bd6f2f4-8b1a-4ffd-966f-06506fd24428	—
Pongo abelii	USNM 143590	?	L	MS	M56324-101610	http://n2t.net/ark:/65665/389dc210f-f5b3-4910-ae87-a26700227801	—
Pongo abelii	USNM 143593	?	L	MS	M56494-101780	http://n2t.net/ark:/65665/329ae2628-4c93-4da7-8e52-5f0c1e7bcc9e	—
Pongo abelii	USNM 143594	?	L	MS	M56426-101712	http://n2t.net/ark:/65665/3a893123e-021c-4f9b-ab42-4b4050332c24	—
Pongo abelii	USNM 143596	?	L	MS	M56423-101709	http://n2t.net/ark:/65665/3c26ea641-6662-42df-9b0d-a288ade0d69c	—
Pongo pygmaeus	AMNH 200900	F	L	AMNH	—	—	NextEngine
Pongo pygmaeus	USNM 142169	F	L	USNM	—	—	NextEngine
Pongo pygmaeus	USNM 145302	F	L	USNM	—	—	NextEngine
Pongo pygmaeus	USNM 153805	F	R	USNM	—	—	NextEngine
Pongo pygmaeus	USNM 153822	F	L	USNM	—	—	NextEngine
Pongo pygmaeus	ZMS 1982-0092	F	R	ZMS	—	—	µCT (BIR ACTIS)
Pongo pygmaeus	USNM 145301	M	L	USNM	—	—	NextEngine
Pongo pygmaeus	USNM 145305	M	L	USNM	—	—	NextEngine
Pongo pygmaeus	USNM 153823	M	L	USNM	—	—	NextEngine
Pongo pygmaeus	ZMS 1909-0801	M	L	ZMS	—	—	µCT (BIR ACTIS)
Pongo pygmaeus	ZMS 1966-0203	M	R	ZMS	—	—	µCT (BIR ACTIS)
Pongo pygmaeus	ZMB 87092	?	L	ZMB	—	—	µCT (BIR ACTIS)
Symphalangus syndactylus	AMNH 106583	F	L	AMNH	—	—	NextEngine
Symphalangus syndactylus	NMNH 271048	F	L	USNM	—	—	NextEngine

Symphalangus syndactylus	AMNH 106581	M	L	AMNH	—	—	NextEngine
Symphalangus syndactylus	PSU 105-1841	?	L	MS	M45351-82643	—	—
Symphalangus syndactylus	UWBM 58721-1	?	R	MS	M69298-125011	—	—
Symphalangus syndactylus	UWBM 82801-1	?	L	MS	M69299-125019	—	—
Symphalangus syndactylus	ZMB 38573	?	R	ZMB	—	—	µCT (BIR ACTIS)
Symphalangus syndactylus	ZMB 38587	?	L	ZMB	—	—	µCT (BIR ACTIS)

Abbreviations: F = female; M = male; ? = unknown sex; L = left; R = right; AMNH = American Museum of Natural History, New York, USA; CMNH = Cleveland Museum of Natural History, Cleveland, USA; MPI-EVA = Max Planck Institute for Evolutionary Anthropology, Leipzig, Germany; MS = MorphoSource.org; PCM = Powell-Cotton Museum, Birchington, UK; RMCA = Royal Museum for Central Africa, Tervuren, Belgium; SBU = Stony Brook University, New York, USA; USNM = Smithsonian National Museum of Natural History, Washington D.C., USA; ZMB = Museum für Naturkunde – Leibniz Institute for Evolution and Biodiversity Science, Berlin, Germany; ZMS = Zoologische Staatssammlung Munchen, Munich, Germany.

SOM Table S2

The meaningful between-group principal component (bgPC1 and bgPC2) scores for the original fossil and a high-quality cast of the proximal radius of *Barberapithecus* (IPS66267). See also SOM Figure S2.

Specimen	bgPC1 scores	bgPC2 scores
IPS66267 (original)	0.10657264	-0.01297840
IPS66267 (cast)	0.10881666	-0.00938558

SOM File S1. 3D model of the right proximal radius (IPS66267) of *Barberapithecus huerzeleri* from Castell de Barberà, available as a PLY file from MorphoSource.org (https://doi.org/10.17602/M2/M349186).